Structural Biology and Molecular Biophysics

A binding site for phosphoinositides described by multiscale simulations explains their modulation of voltage gated sodium channels

Yiechang Lin ✉, **Elaine Tao** ✉, **James P Champion**, **Ben Corry** ✉

Research School of Biology, Australian National University, Canberra

Reviewed Preprint

Revised by authors after peer review.

About eLife's process

Reviewed preprint version 2
February 20, 2024 (this version)

Reviewed preprint version 1
October 5, 2023

Sent for peer review
July 28, 2023

Posted to preprint server
July 17, 2023

Abstract

Voltage gated sodium channels (Na_v) are membrane proteins which open to facilitate the inward flux of sodium ions into excitable cells. In response to stimuli, Na_v channels transition from the resting, closed state to an open, conductive state, before rapidly inactivating. Dysregulation of this functional cycle due to mutations causes diseases including epilepsy, pain conditions and cardiac disorders, making Na_v channels a significant pharmacological target. Phosphoinositides are important lipid cofactors for ion channel function. The phosphoinositide $PI(4,5)P_2$ decreases $Na_v1.4$ activity by increasing the difficulty of channel opening, accelerating fast inactivation and slowing recovery from fast inactivation. Using multiscale molecular dynamics simulations, we show that $PI(4,5)P_2$ binds stably to inactivated Na_v at a conserved site within the DIV S4-S5 linker, which couples the voltage sensing domain (VSD) to the pore. As the Na_v C-terminal domain is proposed to also bind here during recovery from inactivation, we hypothesise that $PI(4,5)P_2$ prolongs inactivation by competitively binding to this site. In atomistic simulations, $PI(4,5)P_2$ reduces the mobility of both the DIV S4-S5 linker and the DIII-IV linker, responsible for fast inactivation, slowing the conformational changes required for the channel to recover to the resting state. We further show that in a resting state Na_v model, phosphoinositides bind to VSD gating charges, which may anchor them and impede VSD activation. Our results provide a mechanism by which phosphoinositides alter the voltage dependence of activation and the rate of recovery from inactivation, an important step for the development of novel therapies to treat Na_v-related diseases.

Significance

Voltage-gated sodium channels form pores in the membrane to mediate electrical activity in nerve and muscle cells. They play critical roles throughout the human body and their dysfunction leads to diseases including epilepsy, cardiac arrhythmias and pain disorders. Membrane lipids called phosphoinositides have recently been shown to reduce the activity of a voltage-gated sodium channel, but the molecular basis of this mechanism is not known. Here we use simulations to reveal where these lipids bind to the channels and how they reduce channel activity by making it harder for the pores to open and slower to subsequently recover to the closed resting state.

eLife assessment

This **important** study employs multiscale simulations to show that PIP2 lipids bind to DIV S4-S5 linkers within the inactivated state of a voltage-gated sodium channel, affecting the coupling of voltage sensors to the ion-conducting pore. The authors demonstrate that PIP2 prolongs inactivation by binding to the same site that binds the C-terminal during recovery from inactivation, and they suggest that binding to gating charges in the resting state may impede activation, both findings that contribute to our understanding of sodium channel modulation. The coarse-grained and atomistic molecular dynamics simulations are **convincing**, including state dependence and linker mutants to back up the claims.

Introduction

Voltage-gated sodium (Na_v) channels are critical to the regulation of brain activity, cardiac rhythm, and muscle contraction. Expressed in the membranes of excitable cells, Na_v channels respond to membrane depolarization to open a pore that facilitates the selective flow of sodium current into the cell, initiating the action potential. In mammals, the Na_v channel family consists of nine subtypes (Na_v 1.1-1.9), distributed throughout the central and peripheral nervous system, as well as in cardiac and skeletal muscle (1). The $Na_v1.4$ subtype is predominantly expressed in skeletal myofibers, where it initiates muscle contraction. Genetic mutations in this subtype are associated with various motor dysfunctions, such as both hyperkalaemic and hypokalaemic periodic paralyses (2-4). $Na_v1.7$ is found in peripheral sensory neurons and is responsible for nociception. Several pain disorders, such as inherited erythromelalgia and small fibre neuropathy arise from gain-of-function $Na_v1.7$ mutations (5). Both Na_v subtypes have been investigated as promising pharmacological targets for the treatment of myopathy and pain conditions (5, 6).

Structurally, Na_v channels consist of four homologous domains (DI-DIV) arranged in a domain-swapped configuration (**Fig. 1A-B**). Each domain comprises of six transmembrane helices (S1-S6). The central pore domain is formed by S5, S6 helices and selectivity filter (SF), while the four peripheral voltage-sensing domains (VSDs) are formed by S1-S4 (7, 8). The pore domain also features lateral fenestrations that provide a pathway for the access of small molecules to the pore via the membrane (9) and have been shown in computational studies to be accessible to lipid tails (10-13). Additionally, the C-terminal domain (CTD) extends from the DIV S6 helix into the cytoplasm, where it is thought to associate with the DIII-IV and DIV S4-S5 linkers in the resting state (14).

Na_v channels adopt distinct functional states during the cycle of membrane depolarization and repolarization (**Fig. 1C**). In the resting state, the pore is closed and VSD S4 helices are in the down, deactivated state. Membrane depolarization triggers the asynchronous transition of VSD I-III S4 helices to the up, activated conformation, causing Na_v channels to open (15-17). During prolonged depolarization, VSD-IV moves upwards, causing the channels to adopt a fast inactivated state in which a three-residue Ile-Phe-Met (IFM) hydrophobic motif located on the intracellular linker between DIII and DIV (DIII-IV linker) allosterically closes the pore (18). The CTD is proposed to bind at the S4-S5 linker of VSD-IV and sequester the DIII-IV linker during the resting state. During fast inactivation, the CTD dissociates from VSD-IV and releases the DIII-IV linker to allow IFM binding (14). Upon repolarization, the VSDs deactivate, the IFM motif disassociates, the CTD rebinds to VSD-IV and the pore returns to the resting state.

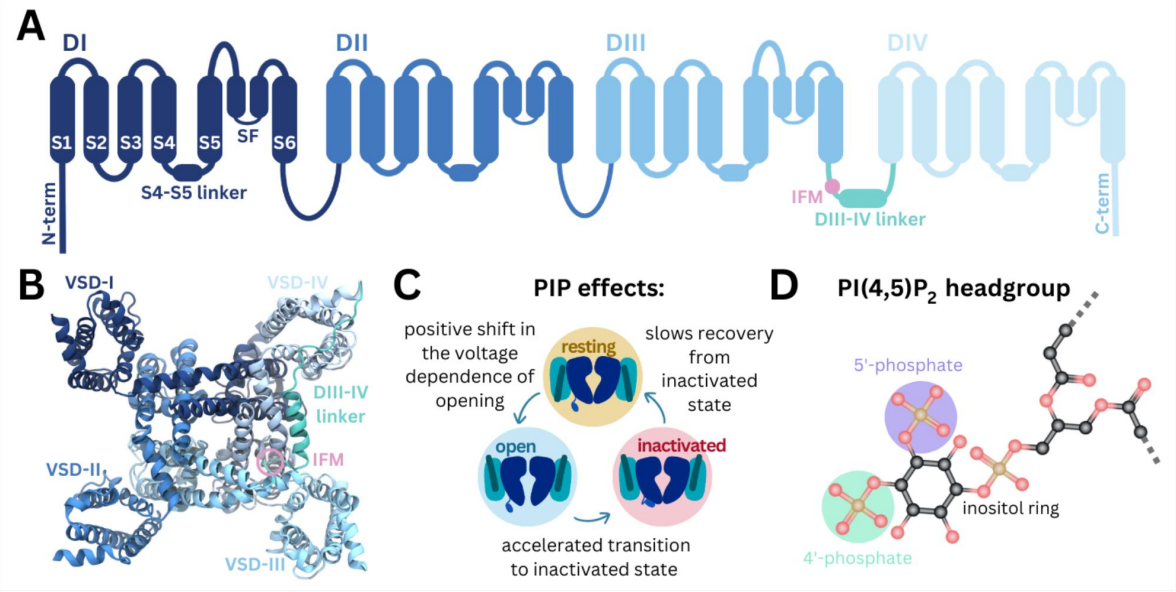

Fig. 1.

Structure of Na_v and modulation by phosphoinositides

(A) Na_v channel topology featuring transmembrane helices (S1-S6), the selectivity filter (SF) and the DIII-IV linker (containing the IFM motif) located between DIII and DIV. **(B)** $Na_v1.4$ structure (6agf) showing the four domain-swapped voltage sensor domains (VSDs I-IV), pore and DIII-IV linker on the intracellular side. **(C)** Summary of $PI(4,5)P_2$ effects on transitions between Na_v channel functional states (25) **(D)** Structure of the $PI(4,5)P_2$ headgroup with the 4'- and 5'-phosphates indicated

Phosphoinositides (PIPs) are important cellular signaling molecules found on the cytoplasmic leaflet of the mammalian cell membrane. They can exist in seven forms, with phosphorylation possible at one (PIP1), two (PIP2) or all three (PIP3) positions on the inositol ring, at the 3', 4' and/or 5' carbons. PIPs, particularly $PI(4,5)P_2$, featuring phosphates at the 4' and 5' carbon positions (**Fig. 1D**), are known to bind and modulate the activity of numerous ion channels families (19). These include voltage-gated ion channels, some of which have been resolved with $PI(4,5)P_2$ bound (20, 21). PIP is known to interact with the VSDs of different potassium channels, to stabilize the positive gating charges and support the voltage-sensing mechanism (22). By also binding at the VSD-pore interface in channels such as $K_v7.1$, PIP is proposed to facilitate coupling of VSD movement to pore opening (20, 23, 24). $PI(4,5)P_2$ also forms specific interactions with VSD-II of $Ca_v2.2$ in the down-state, making channel activation more difficult (21). Although $PI(4,5)P_2$ is known to bind to numerous voltage gated ion channels, its effects on channel gating and function are complex and yet to be fully elucidated.

Recent experiments show that $Na_v1.4$ channel kinetics and voltage dependence are modulated by $PI(4,5)P_2$ (25). $PI(4,5)P_2$ inhibits $Na_v1.4$ by causing a depolarizing shift in voltage dependence of activation, accelerating transition to the inactivated state and slowing recovery from inactivation, resulting in reduced peak current and suppression of late current (summarized in **Fig. 1C**). While this is likely to occur via a direct interaction with $Na_v1.4$, the structural basis of $PI(4,5)P_2$ modulation remains to be understood.

Here, we used a combination of coarse-grained and atomistic MD simulations to identify a putative PIP binding site to inactivated $Na_v1.4$ in VSD-IV and the DIII-IV linker. We analyze the atomistic level interactions between the positively charged residues at this site with $PI(4,5)P_2$ and PI(4)P, comparing this with structurally resolved PIP binding sites in the related ion channels $Ca_v2.2$ and $K_v7.1$. Consistent with the sequence conservation at the identified site, we find that PIPs also bind to $Na_v1.7$ in coarse-grained simulations, with notable differences dependent on VSD conformation states. This work provides insight into how PIPs can negatively regulate Na_v channels, a first step for the potential development of PIP-analogue sodium channel inhibitors.

Results

To investigate how diverse lipid species interact with $Na_v1.4$, we carried out coarse-grained simulations of $Na_v1.4$ (PDB ID: 6agf, inactivated state) embedded in a complex mammalian membrane for 16 μs in triplicate (**Fig. 2A**). Glycosphingolipid (GM), phosphoinositide (PIP) and diacylglycerol (DAG) were highly enriched around $Na_v1.4$ (**Fig. 2B**). Additionally, we observed modest enrichment of lysophosphatidylcholine (LPC), phosphatidylinositol (PI), phosphatidylserine (PS) and phosphatidylethanolamine (PE) and slight depletion of ceramide (CER), sphingomyelin (SM), phosphatidylcholine (PC) and cholesterol (CL). To investigate specific interactions, we generated z-density maps and calculated the per-residue occupancy of the 12 different lipid types (**Fig. 2C**, Fig. S1-2). Binding residues of interest were identified by constructing occupancy distributions by residue for each lipid type and identifying outlying values with high occupancies (Fig. S3). DG lipids form significant interactions within the lateral fenestrations of $Na_v1.4$ (Fig. S2). LPC and PI also frequently interact with different VSD residues (Fig. S1).

Given our interest in understanding the modulation of $Na_v1.4$ by PIPs, we focus on their interactions for the remainder of this manuscript. Despite the very low concentration of PIPs (0.5% each of PIP1, PIP2 and PIP3) in the mammalian membrane, they are highly enriched around $Na_v1.4$, particularly near the DIII-IV linker and the VSD-IV (**Fig. 2C**). Contact analysis revealed a putative PIP binding site involving the K1330 residue of the DIII-IV linker and residues R1463, K1466 and R1469 in the DIV S4-S5 linker, which connects the pore and VSD-IV (**Fig. 2D**). Across all three replicates, only residues within this site were occupied by PIPs for more than 80%

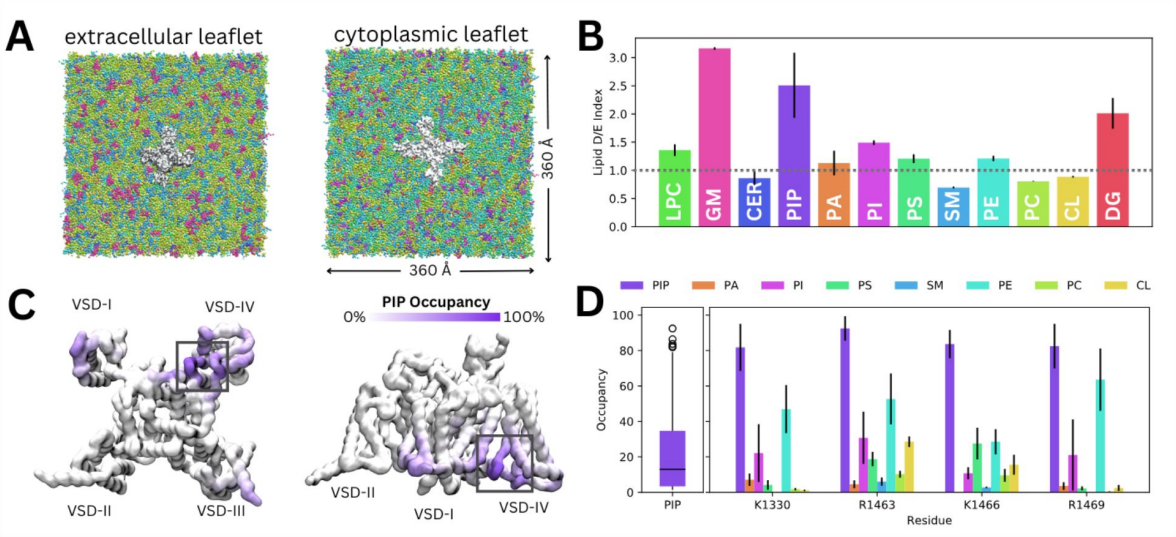

Fig. 2.

Lipid fingerprint and binding of all PIP types to $Na_V1.4$

(A) $Na_V1.4$ embedded in a 360 Å x 360 Å model mammalian membrane containing 63 lipid species. **(B)** Lipid depletion enrichment index of lipids around $Na_V1.4$ grouped into 12 headgroup classes **(C)** $Na_V1.4$, shown from the intracellular (left) and membrane (right) sides, colored by PIP occupancy (darker purple = greater PIP occupancy) **(D)** Distribution of PIP binding occupancies (left) and occupancy of lipid species at 4 residues with the highest PIP occupancy.

(Quartile 3 + 1.5 x Interquartile range) of simulation time on average (**Fig. 2D**). We note that these residues have higher occupancies for PIP compared to other lipids, including other negatively charged phospholipids (PA, PS and PI) (**Fig. 2D**).

Simulations in a complex mammalian membrane showed that PIP species bind specifically and selectively to $Na_V1.4$ in the presence of other negatively charged lipids and at low, physiological concentrations. However, the large membrane required, and long PIP binding durations prevented sampling of large numbers of binding and unbinding events. To address this, we carried out additional simulations where $Na_V1.4$ was placed in a smaller POPC membrane with a 5% concentration of each PIP species in the cytoplasmic leaflet (**Fig. 3A**).

Across ten replicates of these enriched PIP simulations, each carried out for 80 μs, we observed all three PIP species binding at the identified site on VSD-IV and DIII-IV linker (**Fig. 3B**). PIPs can approach and bind to this site from either side of the VSD, however, PIP1 only forms stable interactions when it approaches and binds from the VSD-I side while PIP2 and PIP3 usually bind from the VSD-III side (**Fig. 3B**). These enriched PIP simulations also revealed additional positively charged residues in the DIII-IV linker (K1329, K1333 and K1352) and DIV S4 (R1460) which support binding.

There were 156 PIP binding/unbinding events with duration greater than 2 μs occurring in the identified site (**Fig. 3C**). Of these, 43 were with PIP1, 44 with PIP2 and 33 with PIP3. The number of short-term (2-10 μs) interactions decreased with headgroup charge. That is, PIP1 formed the greatest number of short-term interactions while PIP3 had the fewest. Of the 31 binding events with duration greater than 10 μs, 7 were with PIP1, 15 with PIP2 and 9 with PIP3 (Fig. S4-5).

When we analyzed interactions occurring during 2-80+ μs binding events, we found that the number of interacting basic residues changes depending on the PIP headgroup charge (**Fig. 3D**). PIP1 (headgroup charge: -3e) binding is most frequently coordinated by two positive charges in VSD-IV and zero or one residue in the DIII-IV linker. PIP2 (headgroup charge: -5e) binding most frequently involves one or two interactions from the DIII-IV linker and three from VSD-IV for a total of five interactions. Interestingly, despite its greater negative charge, PIP3 (headgroup charge: -7e) interacts similarly to PIP1, and has fewer interactions than PIP2.

The minimum distance between the interacting PIP headgroup and each binding residue across simulation time is shown for the five 40+ μs PIP binding events (**Fig. 3E**). Of these, three are PIP2 binding events which almost span the entire 80 μs of simulation. One 40+ μs binding event each for PIP1 and PIP3 were also observed. The stable PIP1 binding event observed involved interactions with R1460 and R1469 in VSD-IV, as well as fluctuating interactions with the four residues of the DIII-IV linker (K1329, K1330, K1333, K1352). The three long term PIP2 binding events observed were similar to each other, mainly stabilized by R1460, R1463 and R1469. As with PIP1, the number and identity of interacting DIII-IV linker residues varied across the span of each simulation and between replicates, owing to the flexibility of the linker. Like PIP2, PIP3 binding was characterized by stable interactions with R1460, R1463 and R1469 (VSD-IV) as well as K1329 and K1330 (DIII-IV linker). *In silico* mutation of the eight residues implicated in PIP binding to leucine (charge neutralization while preserving sidechain size) or glutamate (charge reversal) significantly reduced PIP binding (Fig. S6).

Coarse-grained simulations enhance sampling by reducing the number of particles, enabling larger time steps and construction of a smoother energy surface. However, this loss of resolution prevents distinction between phosphate positions on the inositol group and does not permit analysis of protein conformational changes induced by PIP binding. To address this, we backmapped representative snapshots from our PIP enriched simulations, where we observed stable, long-term binding events between $Na_V1.4$ and PIP1/PIP2.

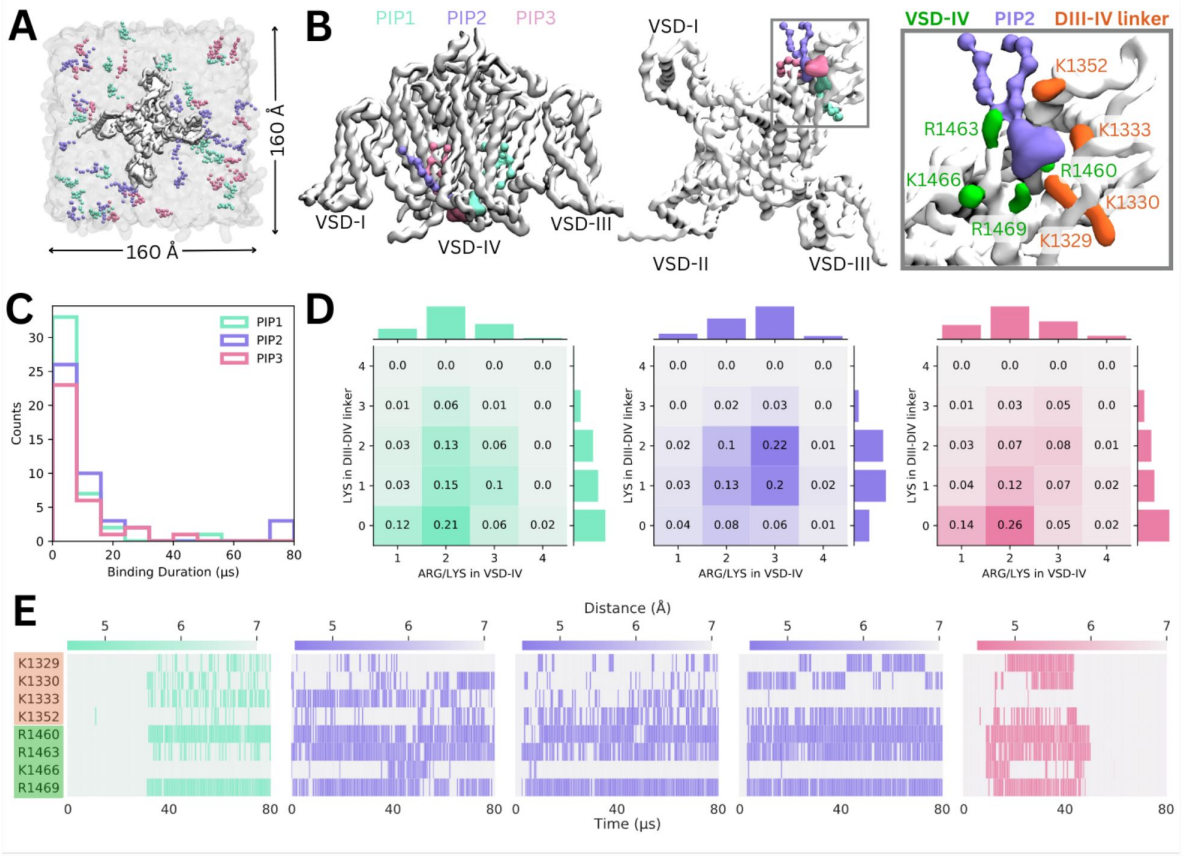

Fig. 3.

Binding of different PIP species in enriched PIP simulations

(A) Enriched PIP simulation system, with $Na_V1.4$ embedded in a POPC membrane (transparent gray) and 5% each of PIP1 (blue), PIP2 (purple) and PIP3 (pink) added to the cytoplasmic leaflet. **(B)** Representative snapshots from the five longest binding events from different replicates, showing the three different PIP species (PIP1 in blue, PIP2 in purple and PIP3 in pink) binding to VSD-IV and the DIII-IV linker. $Na_V1.4$ is shown in white with interacting residues on the DIV S4-S5 linker and the DIII-IV linker colored in green and orange respectively. **(C)** A frequency distribution showing interaction times for each PIP species, defined as the length of a continuous period in which a PIP was within 0.7 nm of two VSD IV binding site residues. **(D)** Frequency plots showing number of positive residues interacting with bound PIP in the DIII-IV linker (vertical) and VSD-IV (horizontal). **(E)** Minimum distance between binding residues on $Na_V1.4$ and bound PIPs lipid across simulation time for the five longest binding events, colored by distance and the type of PIP bound.

The coarse-grained PIP1 and PIP2 molecules were converted to the atomistic PI(4)P and $PI(4,5)P_2$ respectively. For each system, 7.5 μs of atomistic simulations were performed (5 replicates, 1.5 μs each).

In these simulations, the $PI(4,5)P_2$ headgroup was stable at the binding site identified in coarse-grain simulations (RMSD <2.2 Å) (**Fig. 4A**, Fig. S7). $PI(4,5)P_2$ binding is predominantly coordinated by R1469 on the DIV S4-S5 linker, as well as R1466 and R1463. In one replicate, $PI(4,5)P_2$ associates with R1460 via the phosphate group (PO4) that connects the headgroup to the PIP tails. The $PI(4,5)P_2$ headgroup also forms electrostatic interactions with K1329 and K1330 in the DIII-IV linker, but forms few contacts with K1333 (**Fig. 4B**, Fig. S8). This loop portion of the DIII-IV linker is highly flexible (Fig. S7), thus the lysine sidechains are able to flip between binding the $PI(4,5)P_2$ headgroup and facing the intracellular space.

The 4'-phosphate formed interactions with residues belonging to the DIII-IV linker (K1329 and K1333) and DIV S4-S5 linker (K1666 and R1469) with similar frequency, in 55-60% of simulation frames (**Fig. 4B**). In contrast, the 5'-phosphate formed contacts with three VSD-IV S4-S5 residues (R1463, K1466 and R1469) in 70-98% of simulation frames and DIII-IV linker residues in 37-48% of frames. Taken together, this data suggests that although the headgroup is flexible when bound, the 5'-phosphate is more important for coordinating VSD-IV S4-S5 residues while the 4'-phosphate associates with both regions of the binding site.

Atomistic simulations of PI(4)P bound from the VSD-III side show that this is also a stable pose (RMSD <2 Å), where the headgroup interacts with the same positively charged residues as seen for $PI(4,5)P_2$ (**Fig. 4A**, Fig. S7). The residues on the S4-S5 linker, R1463, K1466 and R1469, predominantly bind to the 4'-phosphate (**Fig. 4B**). Due to the more buried location of PI(4)P binding, the PO4 phosphate can associate more with DIII-IV linker lysines (**Fig. 4B**), however, the absence of the 5'-phosphate leads to a reduced number of total electrostatic interactions (Fig. S9).

To investigate structural changes that might occur in the presence of PI(4)P/$PI(4,5)P_2$, we also carried out simulations of the inactivated $Na_v1.4$ structure without any PIPs bound for comparison. Although the DIII-IV linker remains bound throughout simulations both with and without PIPs, residues P1336 and R1337 in the DIII-IV linker downstream of the IFM motif are significantly less mobile with $PI(4,5)P_2$ present (**Fig. 4C**). Additionally, seven residues belonging to the DIV S4-S5 linker, including binding residues K1466 and R1469, also have significantly lower mobility when $PI(4,5)P_2$ is bound (**Fig. 4C**). In the PI(4)P bound simulations, there were no significant differences in DIII-IV linker or S4-S5 linker mobility.

To further probe whether PIP can stabilize the DIII-IV linker and the inactivation gate, we applied coarse-grained simulations with the DIII-IV linker unrestrained. In simulations of WT Nav1.4, the IFM has a reduced stability within its binding pocket when PIP is excluded from the membrane (**Fig. 4E**). To accentuate this effect we simulated an inactivation-deficient variant of Nav1.4, where the IFM motif is mutated to IQM (26). We find that the IQM motif has a greater probability of being tightly associated with the receptor pocket in the presence of PIP compared to without it (**Fig. 4E**), supporting our observation that PIP can stabilize the channel in the inactivated state. This suggests that the presence of PIP may partially rescue some of the structural defects associated with inactivation dysfunction in Nav mutants.

The PIP binding poses seen in our simulations is similar to resolved binding poses for $PI(4,5)P_2$ in cryo-EM structures of $Ca_v2.2$ and $K_v7.1$ (**Fig. 5A**). A sequence alignment of $Na_v1.4$ VSDs show that there are more positively charged residues present in the S4/S4-S5 linker regions of DIV compared to the other domains (**Fig. 5B**). PIP is bound at similar VSD residues on both these ion channels, with PIP forming interactions with a gating charge further up the S4 helix in $Ca_v2.2$ due

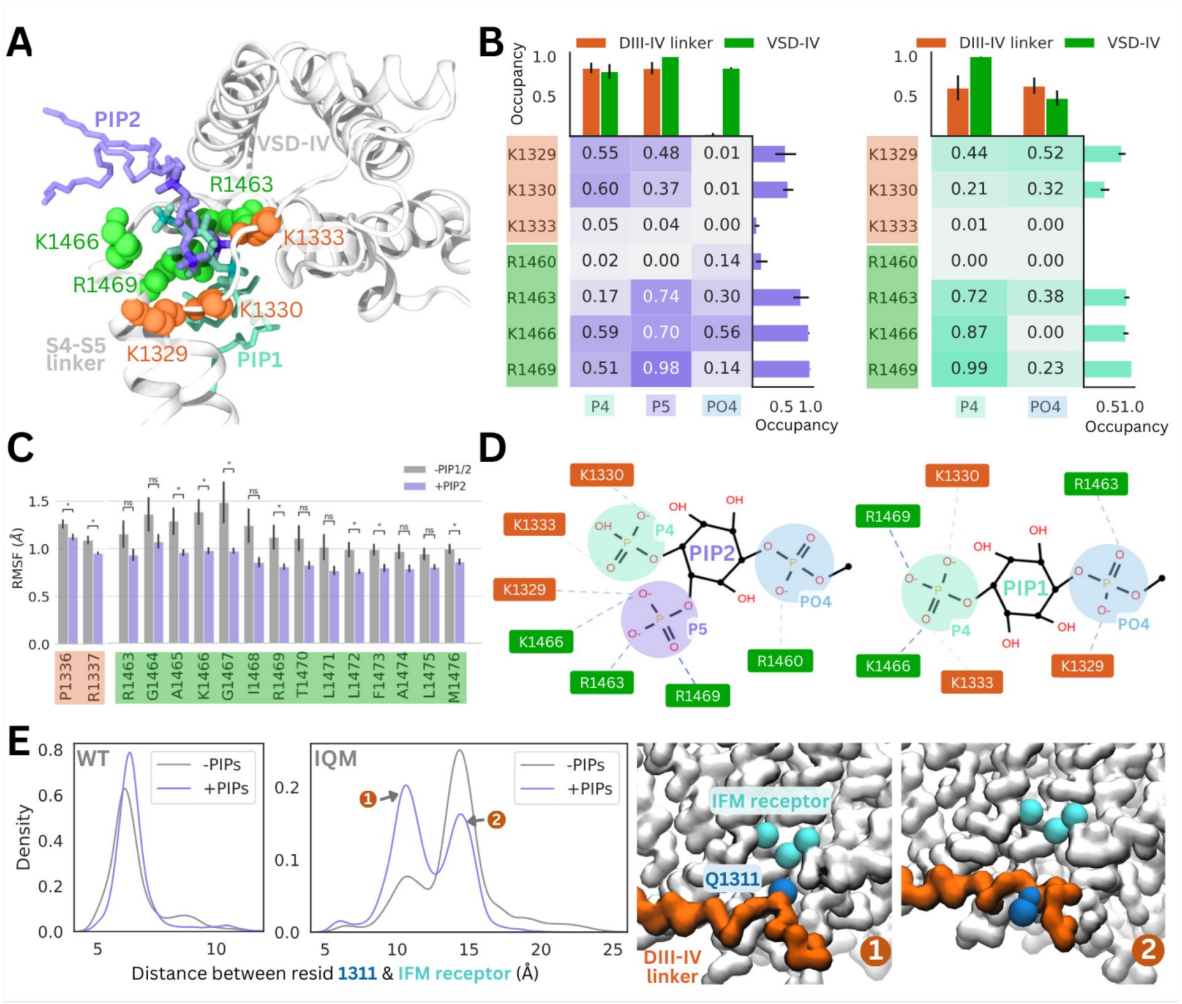

Fig. 4.

PI(4,5)P_2 and PI(4)P binding to $Na_v1.4$ stabilizes the DIII-IV linker in atomistic and flexible coarse-grained simulations

(A) Representative snapshots of PI(4,5)P_2 bound from the VSD-I side (purple stick) and PI(4)P bound from the VSD-III side (cyan stick), with six basic residues forming the binding site located on the DIII-IV linker (orange VDW representation) and VSD-IV S4-S5 linker (shown in green VDW representation) visualized from the intracellular face of the protein **(B)** Proportion of frames where each of the binding site residues were identified to be within 4.5 Å with the different headgroup regions, P4, P5 and PO4, for PI(4,5)P_2 (left) and PI(4)P (right) **(C)** Comparison of RMSF per carbon-alpha for simulations with and without bound PI(4,5)P_2, showing residues on the S4-S5 linker and DIV linker with significant differences in mobility (p-value < 0.05) **(D)** Interaction network plots between the PIP headgroup and basic binding residues on DIII-IV linker (orange) and DIV S4-S5 linker (green), generated by ProLIF – showing the dominant interactions across simulations of PI(4,5)P_2 and PI(4)P. **(E)** Density plots showing differences in the distributions of distance between IFM/IQM motif and its binding pocket in the presence and absence of PIPs for the Nav1.4 wild-type (left) and IFM->IQM mutant (right); with representative snapshots showing the two distinct conformations of the IQM motif in the mutant.

to the VSD being in a different state. Additionally, the high sequence similarity in the S4/S5-S5 linker and DIII-IV linker regions between the nine human Na_v channel subtypes suggests conservation of the PIP binding site (**Fig. 5C**).

To assess possible state- and subtype-dependent differences in PIP binding, we simulated three structures of $Na_v1.7$ with different VSD conformations in a PIP enriched membrane (**Fig. 6A**). The inactivated $Na_v1.7$ structure (blue, PDB ID: 6j8g) contains all VSDs in the activated/up state and a bound DIII-IV linker. We also simulated a Na_vPas (American cockroach) chimera structure with a human $Na_v1.7$ VSD-IV in the deactivated/down state (VSDs I-III are activated, and from Na_vPas) (pink, PDB ID: 6nt4). This structure (14) features a dissociated DIII-IV linker and a resolved C-terminal domain bound to the DIV S4-S5 linker (forming the 'inactivation switch') at residues identified to form part of our PIP binding site. To assess PIP binding at VSD I-III in the deactivated/down state, we modelled the $Na_v1.7$ resting state based on templates structures in which different VSDs have been captured in deactivated states with the aid of toxins (detailed in Table S2). These structures feature three or more of the gating charge residues below the hydrophobic constriction site (HCS) and displacement of the S4-S5 linker (Fig. S10). Given that no resting state mammalian Na_v channel structure has been resolved, it is possible that the modelled VSDs may not reflect the fully deactivated state.

In triplicate 50 μs coarse-grained simulations, PIPs bind to the analogous site to that seen in inactivated $Na_v1.4$ in the inactivated $Na_v1.7$ structure, interacting with residues belonging to both the DIII-IV linker and VSD-IV for durations comparable to $Na_v1.4$, (**Fig. 6B-C**, Fig. S11). Binding of PIP to the DIV S4-S5 linker to the deactivated VSD-IV in the $Na_v1.7$-Na_vPas chimera and resting state model was also observed (**Fig. 6B-C**). However, in the $Na_v1.7$-Na_vPas chimera, the PIP bound at the S4-S5 linker cannot simultaneously associate with the DIII-IV linker (Fig. S11), due to its sequestration by the C-terminal domain, which moves the lysines away from the binding VSD-IV residues (**Fig. 6D**). Instead, K1491, K1492 and K1495 (on the DIII-IV linker) are occupied by different PIPs on the other side of the VSD. In the resting state model, which features an unbound DIII-IV linker PIPs binding at the DIV S4-S5 residues also do not associate with the DIII-IV linker (Fig. S11). Comparison of binding durations at this site across the three systems reveals a greater number of long PIP interactions (> 20 μs) with inactivated $Na_v1.7$ (5) compared to $Na_v1.7$-Na_vPas (3) or the resting state model (2) where VSD-IV is down, and the DIII-IV linker is dissociated.

There are state-dependent differences in PIP occupancy at the gating charges in each VSD (**Fig. 6E-F**, Fig. S12A-B). PIP can associate with the lowest three gating charges VSD-I of the resting state model, but not in the inactivated state (**Fig. 6E**). This is likely due to the large displacement in the DI-S4 helix, which moves down three helical turns in the resting state model so that all gating charges are below the HCS (Fig. S10). In VSD II and III, the PIP interaction differences between inactivated and resting state are present but less pronounced, owing to a smaller difference in the relative displacement between the gating charges between states (Fig. S10). PIP occupancy is also higher at VSD-IV when it is in the deactivated conformation however, the presence of a bound CTD as seen in the $Na_v1.7$-Na_vPas model, reduces this occupancy of PIP (**Figure 6E**). Additional simulations of a resting state model of Nav1.4 built using our Nav1.7 resting state model as a template suggest that similar gating charge interactions occur for Nav1.4 when the VSDs are deactivated (Fig. S12C).

Discussion

Recently, $PI(4,5)P_2$ was shown to be a negative regulator of $Na_v1.4$, modulating channel kinetics and voltage dependence. Presence of $PI(4,5)P_2$ causes a depolarizing shift in the voltage dependence of activation, that is a stronger stimulus is required to produce $Na_v1.4$ opening.

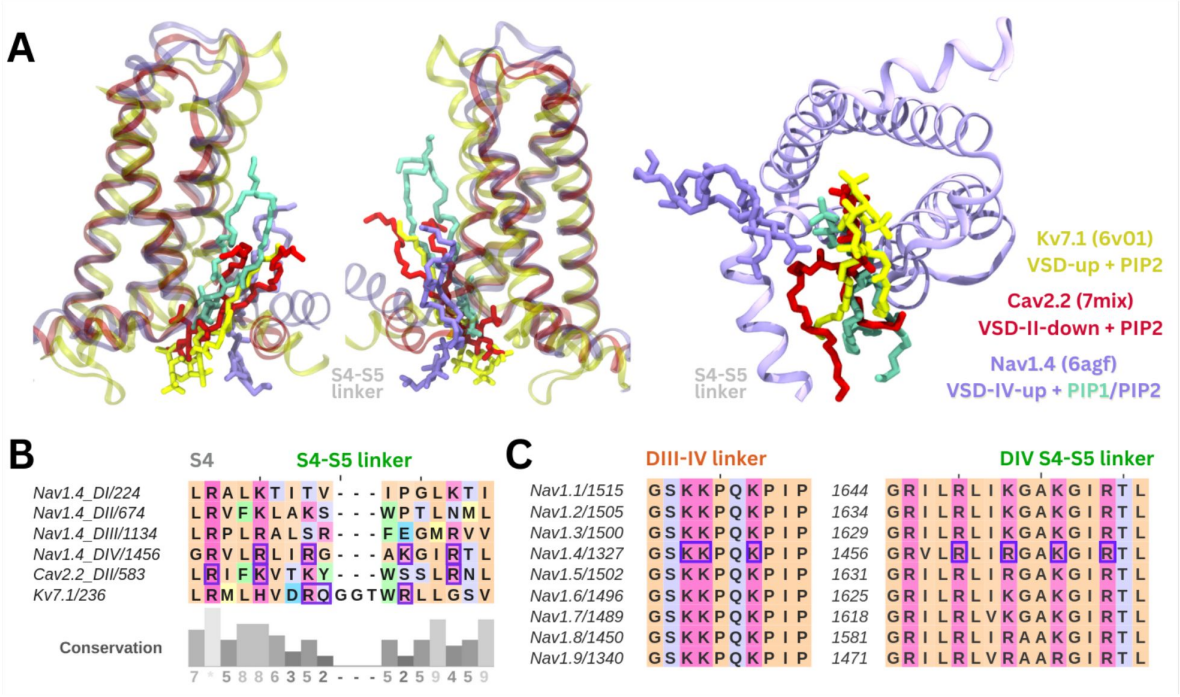

Fig. 5.

Comparison of the identified phosphoinositide binding site to Na_v subtypes and other ion channels

(A) Binding poses of $PI(4,5)P_2$ (in purple) and PI(4)P (in cyan) aligned with two other tetrameric channels structures $K_v7.1$ (6v01, in yellow) and $Ca_v2.2$ (7mix, in red) that were resolved with $PI(4,5)P_2$ at their respective VSDs. **(B)** Sequence alignment of the S4 helix and S4-S5 linker of the four domains of $Na_v1.4$, compared to VSD-II of $Ca_v2.2$ and one of the four identical VSDs of $K_v7.1$; residues colored by amino acid class; purple boxes indicate $PI(4,5)P_2$ binding residues (identified with 5 Å of the headgroup). **(C)** Sequence alignment of the nine human Na_v channel subtypes shows high sequence similarity in the S4 helix, S4-S5 linker and DIII-IV linker regions.

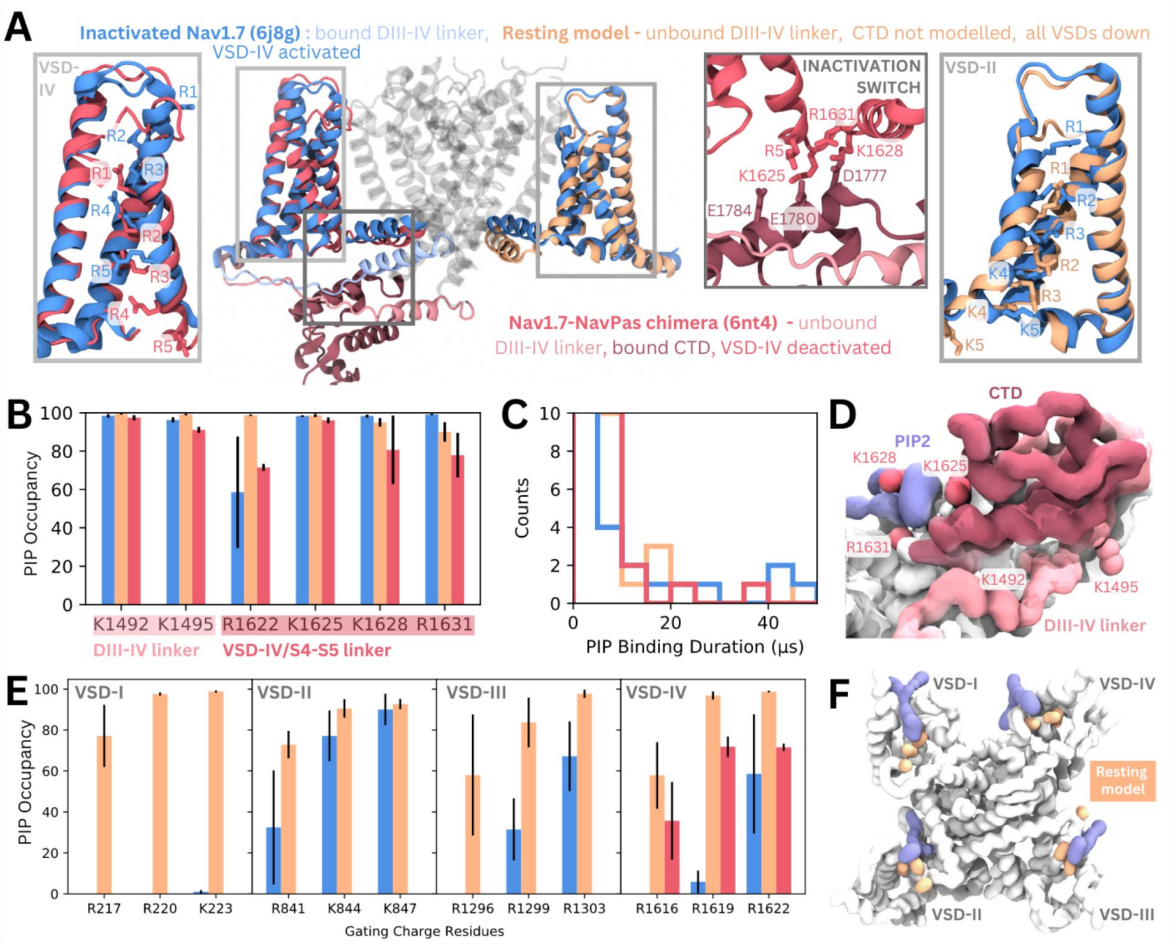

Fig. 6.

PIP binding to $Na_V1.7$ with different VSD states in coarse-grained simulations

(A) Atomistic representation of the three different $Na_V1.7$ structures simulated: (1) the inactivated state (blue, PDB ID: 6j8g) with the VSDs all in the activated, up state (2) the $Na_V1.7$-Na_VPas chimera (pink, PDB ID: 6nt4) with the $Na_V1.7$ VSD-IV in the deactivated, down state and a bound Na_VPas CTD (3) a $Na_V1.7$ resting state model (orange, model generation detailed in Table. S2) with all four VSDs in the deactivated, down state. Panel insets show the different conformations of VSD-IV (left) and VSD-II (right) across different structures. The inactivation switch formed by the CTD and VSD-IV S4-S5 linker proposed by Clairfeuille et al. is shown (middle). **(B)** Combined occupancy of all PIP species (PIP1, PIP2, PIP3) at binding site residues in the three systems **(C)** Distribution of PIP binding durations at the identified site **(D)** Intracellular view of CTD covering the resting state VSD-IV. Representative snapshot of PIP binding at DIV S4-S5 linker in the $Na_V1.7$-Na_VPas system. The CTD (dark pink) prevents PIP access to DIII-IV linker lysines, K1492 and K1495. **(E)** Combined PIP occupancy at the bottom three gating charges on VSD I-III in the inactivated (blue) and resting state model (orange) simulations. For VSD-IV, PIP occupancy in the $Na_V1.7$-Na_VPas system (pink) is also shown. **(F)** Representative simulation snapshot showing PIP (purple) binding at the gating charges (orange) in the resting state model simulations.

Additionally, it stabilizes the inactivated state of $Na_v1.4$, marked by both shortened times to inactivation and slowed recovery from the inactivation.

Using a multiscale simulation approach, we identified a putative PIP binding site comprised of positively charged residues belonging to the S4 helix/S4-S5 linker of VSD-IV (R1460, R1463, K1466, R1469) and DIII-IV linker (K1329, K1330, K1333, K1352). Coarse grained simulations of $Na_v1.4$ embedded in a complex membrane showed that PIP interacts with residues belonging to VSD-IV and the DIII-IV linker. In coarse grained enriched PIP simulations, PIP2 formed longer duration interactions with $Na_v1.4$ than PIP1 and PIP3, supported by a greater number of charged interactions. Atomistic simulations verified the stability of $PI(4,5)P_2$ (the most common PIP2 species in the plasma membrane) at this site and showed that the binding of $PI(4,5)P_2$ reduces the mobility of some DIV S4-S5 and DIII-IV linker residues. Simulations of $Na_v1.7$ with VSDs in different conformational states showed that the PIP binding site is conserved in $Na_v1.7$ and that PIP interactions at VSD gating charges are functional state dependent, with more interactions being formed when the VSDs are deactivated.

The DIII-IV linker, CTD and S4-S5 linkers all play key roles throughout the Na_v conformational cycle. Mutation of the IFM inactivation motif as well as other residues in the DIII-IV linker alter fast inactivation and recovery from fast inactivation (27, 28). While the precise role of the Na_v C-terminal domain and its conformation during the Na_v activation cycle remain elusive, it is likely to be important for coordinating fast inactivation (14, 29). CTD binding to DIV S4-S5 and sequestration of the DIII-IV linker is proposed to occur in the resting state. After the pore opens, activation of VSD-IV is thought to cause CTD dissociation, releasing the DIII-IV linker to allow fast inactivation. Residues in 'switch 1' of the CTD-binding site on the DIV S4-S5 stably bind PIP in our simulations of inactivated $Na_v1.4$ and $Na_v1.7$. We hypothesize that PIP binding at this location makes it more difficult for the CTD to reassociate with VSD-IV, a conformational change which is required during recovery from inactivation.

More generally, the S4-S5 linkers in all four domains couple the VSD to the pore helices and adopt different orientations depending on VSD activation states. When the VSD is activated (in the open and inactivated states), the S4-S5 linkers lie parallel to the membrane. In the resting state, when the voltage sensor is deactivated, the S4-S5 linkers move downward below the plane of the membrane. We propose that PIP binding at the identified site could additionally stabilize both the DIV S4-S5 linker and DIII-IV linker to favor the inactivated state. Although the recovery from fast inactivation occurs on the order of several milliseconds (30), and is beyond atomistic simulation timescales, we observed statistically significant reductions in the RMSF of several DIII-IV linker and DIV S4-S5 linker residues when $PI(4,5)P_2$ was bound in 1.5 μs atomistic simulations. Reduction in the mobility of the DIII-IV linker may slow the dissociation of the upstream IFM motif and stabilization of the S4-S5 linker prevents the downward movement required for the channel to transition back to the resting state.

The PIP binding residues identified here are conserved in $Na_v1.1$-1.9 (**Fig. 5C**), suggestive of a shared binding site and mechanism for PIP-mediated modulation across subtypes. Mutations at these conserved residues in other subtypes lead to various gain-of-function diseases (Table S1). For example, analogous to the $Na_v1.4$ R1469 residue, the R1642C mutation (in $Na_v1.3$) leads to developmental epileptic encepahlopathy (31), and R1644C/H mutations in $Na_v1.5$ (analogous to R1469 in $Na_v1.4$) cause cardiac arrythmias, characterized by accelerated rates of channel recovery from inactivation (32). Consistent with our observations, these diseases with mutations on the DIII-IV linker are likely to reduce $PI(4,5)P_2$ binding, which could be a contributing factor to instability of inactivated state in these pathogenic variants. These inactivation-deficient variants, as well as the IQM variant that we simulated, further emphasize that interactions between $PI(4,5)P_2$ with Na_v channels could be important for prolonging the fast-inactivated state.

The PIP binding site identified here harbors sequence and structural similarity to $PI(4,5)P_2$ binding sites found in other cation channels (**Fig. 5B**). For example, $PI(4,5)P_2$ is resolved at a similar site near the VSD and S4-S5 linker in a recent cryo-EM structure of $K_v7.1$, where the phosphate headgroup forms analogous contacts to R249 and R243 (PDB ID: 6v01) (20). Despite differences in the role of $PI(4,5)P_2$, which negatively regulates $Na_v1.4$ but is required for $K_v7.1$ pore opening, the binding site appears to be conserved. Based on the $PI(4,5)P_2$ binding site, a structurally similar compound was developed as an activator of K_v7 channels and proposed to be a future antiarrhythmic therapy (33).

$PI(4,5)P_2$ also binds to the down, deactivated state of VSD-II in $Ca_v2.2$ (PDB ID: 7mix) (21). In this structure, the $PI(4,5)P_2$ headgroup interacts with two VSD-II gating charges, R584 and K587. Compared to the positioning of $PI(4,5)P_2$ in our simulations of $Na_v1.4$ with an activated VSD-IV, the headgroup associates further up the S4 helix in $Ca_v2.2$ due to the VSD being in a deactivated state. This is also seen in $K_v7.1$ which contains an extended GGT loop in the S4-S5 linker which prevents $PI(4,5)P_2$ binding in the VSD-down state (34). In our coarse-grained simulations of the resting $Na_v1.7$ model, we observe a similar state-dependent difference in $PI(4,5)P_2$ interactions with the deactivated states of each VSD. Since activation of VSDs I-III are known to be coupled to channel opening (17), we propose that PIP binding at these VSDs impedes their ability to activate and thus increases the voltage threshold required of opening. $PI(4,5)P_2$ binding at VSD-IV is prevented by presence of the CTD (and absence of the DIII-IV linker) in the resting state, thus not affecting the kinetics of inactivation onset.

The leftward shift in voltage dependence of inactivation is less pronounced when $PI(4,5)P_2$ is converted to PI(4)P rather than completely dephosphorylated to PI (25). This suggests that PI(4)P may play a compensatory role when $PI(4,5)P_2$ is not present. This is supported by our simulations which show that PI(4)P can also stably occupy the identified binding site, albeit with shorter duration and form less electrostatic interactions compared to $PI(4,5)P_2$. Our atomistic simulations also showed that the 5'-phosphate is more important than the 4'-phosphate for forming interactions with the DIV S4-S5 linker residues of the inactivation switch. These factors suggest that $PI(4,5)P_2$ binding is preferred over PI(4)P at this site and can better compete to bind over the CTD, implying that $PI(4,5)P_2$ is more effective at stabilizing the inactivated state and inhibiting recovery to the resting state.

Simulations using the Martini2.2 forcefield have previously been used to investigate lipid-protein interactions (35) and successfully predict specific lipid binding sites, including the PIP binding site on Kir channels (36). While Martini2.2 simulations explicitly represent all three PIP species (PIP1, PIP2 and PIP3) present in the mammalian membrane, the beads do not distinguish between phosphate positions within each charge state (e.g. $PI(3,4)P_2$ vs $PI(4,5)P_2$). While they can be parameterized for a specific sub-species, we instead employed atomistic simulations to complement and strengthen findings from coarse grain simulations, allowing us to identify the specific contribution of the 4'- and 5'-phosphate groups to binding as well as investigate the conformational changes associated with $PI(4,5)P_2$ binding. Since the precise protonation of the $PI(4,5)P_2$ headgroup in a physiological setting is unclear, we explore one case with the 4'-phosphate protonated. Given that the $PI(4,5)P_2$ headgroup can adopt slightly different binding orientations and can fluctuate over the course of atomistic simulations (Fig S8), we expect the alternate protonation state to have similar affinity for the binding site.

In this work we made use of the Martini2.2 model for our coarse-grained simulations, however recently the refined Martini3 (37) has become available and will be a useful tool for further interrogating protein-lipid interactions, as a greater number of lipid parameters become available. Our coarse-grained simulations also allow us to investigate the association of other lipid types with Nav1.4. While we focus on PIP here, there are other lipid species that have modulatory effects on Nav channels, such as cholesterol (38), glycolipids, DG, LPC and PI, and their interactions warrant further investigation.

Conclusion

Using multiscale simulations, we show that PI(4,5)P_2 binds stably to inactivated structures of $Na_v1.4$ and $Na_v1.7$ at a conserved site within the DIV S4-S5 linker. As the CTD is proposed to also bind here during recovery from inactivation, we hypothesize that PI(4,5)P_2 competes with the CTD to bind to this site, prolonging inactivation. At this site, PI(4,5)P_2 simultaneously binds to the DIII-IV linker which is responsible for allosterically blocking the pore during fast inactivation (**Fig. 7**). Its binding reduces the mobility of both the DIV S4-S5 and DIII-IV linkers, potentially slowing the conformational changes required for the channel to recover to the resting state. We also propose that in the resting state, PIPs form additional interactions with S4 gating charges, particularly in VSD-1, anchoring them to the membrane in a way which may make the upwards movement required for their activation more difficult. Our results provide insight into how sodium channels are modulated by phosphoinositides, an important step for the development of novel therapies to treat Na_v-related diseases.

Methods

Coarse grained simulations

Coarse-grained simulations of $Na_v1.4$ embedded in a complex mammalian membrane were carried out to investigate lipid-protein interactions. The inactivated $Na_v1.4$ alpha subunit (PDB ID: 6agf) (8) was coarse-grained using the CHARMM-GUI Martini Maker (39, 40) and embedded in a 360 Å x 360 Å complex membrane using insane.py (41). The composition of the complex mammalian membrane is as reported in Ingólfsson, *et al.* (42). Three replicate simulations, each with different starting coordinates, were carried out for 16 μs each.

To better sample binding events, we also carried out PIP-enriched simulations in which $Na_v1.4$ was embedded in a 160 Å x 160 Å POPC membrane with 5% of each PIP species, PIP1, PIP2, PIP3 (with charge parameters of -3e, -5e and -7e respectively), added to the cytoplasmic leaflet using insane.py. Ten replicate simulations, each with different starting coordinates, were carried out for 80 μs each. To validate our proposed binding site, we additionally mutated the positively charged PIP binding site residues K1329, K1330, K1330, K1352, R1460, R1463, K1466 and R1469 to leucines ('8L') or glutamates ('8E) and simulated these mutant channels in enriched PIP membranes for 20 μs in triplicate. To explore the possibility for PIP to stabilize the DIII-IV linker in an inactivation-deficient Nav1.4 variant, additional coarse-grained simulations were carried out where the DIII-IV linker region (residues L1305-K1341) was unrestrained for both the WT Nav1.4 and simulations in which the IFM motif was mutated to IQM. In these simulations, an elastic network was applied to E1314-G1327 in the linker to preserve the helicity of this region. Flexible linker simulations were conducted in triplicate for 20 μs in both PIP-enriched bilayers and POPC-only bilayers.

To explore possible state and subtype dependent differences in PIP binding, the inactivated $Na_v1.7$ structure (PDB ID: 6j8g) (43) and the $Na_v1.7$-Na_vPas chimera with CTD bound and VSD-IV in the deactivated state (PDB ID: 6nt4) (14) were also coarse-grained and simulated in PIP-enriched membranes (same protocol as above) for three replicates of 50 μs each. Additionally, a model $Na_v1.7$ with all four VSDs in the deactivated state was built using Modeller (44) and simulated in triplicate for 50 μs each. The template and structural information for this model are detailed in Table S2. In brief, VSD-I down was modelled from 7xve (45), VSD-II and VSD-III were both modelled from the deactivated VSD-II from 7k48 (46), and VSD-IV and the unbound DIII-IV linker were modelled from the corresponding regions in 6nt4 (14). Adjacent S5/S6 regions to each VSD were also modelled from each specified template to ensure proper contacts between the

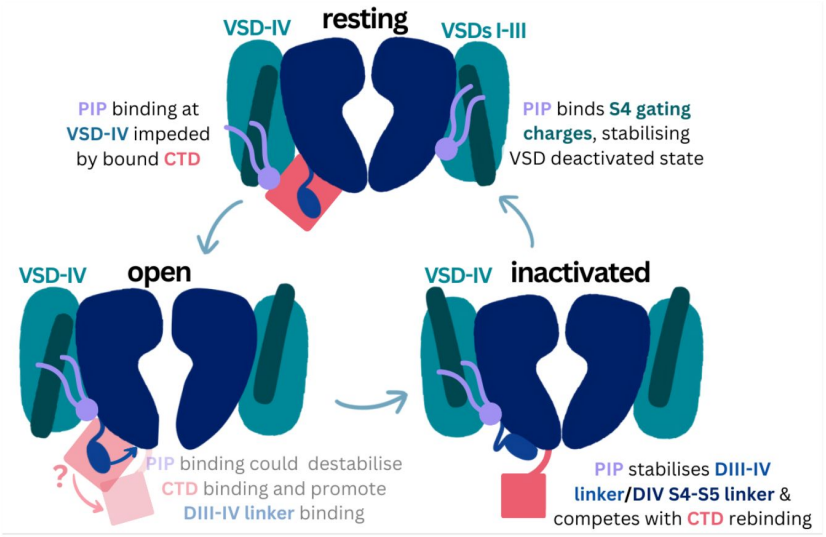

Fig. 7.

Proposed mechanism of PIP effects on the sodium channel functional cycle

pore domain and VSDs. The CTD was not included in the model. Using these $Na_v1.7$ templates, the resting state model of $Na_v1.4$ was generated and simulated for three replicates in coarse grain with the protein backbone restrained, in a PIP-enriched membrane for 50 μs.

All systems were solvated and ionized with 150 mM NaCl. All coarse-grained simulations were carried out with GROMACS 2022 (47) using the Martini2.2 forcefield (48) and the default PIP parameters for each charge state (where PIP2 is based on PI(3,4)P2). Energy minimization was carried out on each system using the steepest descent method for 1,000 steps. Following this, equilibration in the constant pressure, constant volume (NVT) ensemble at 1 atm for 10 ps was carried out with backbone position restraints (1,000 kJ $mol^{-1}nm^{-2}$) using a 2-fs timestep. Following this, constant pressure and temperature (NPT) equilibration simulations were carried out, using 5-, 10-, and 20-fs timesteps in sequence, with each running for 5,000 steps. 1 atm pressure was maintained using a Berendsen barostat with semi-isotropic conditions. Production simulations were carried out in the NPT ensemble, kept at a temperature of 310 K using the Nose-Hoover thermostat (49) and a pressure of 1 bar using the Parrinello-Rahman barostat (50). A time step of 20 fs was used. During production simulations, the backbone beads were weakly restrained to their starting coordinates using a force constant of 10 kJ $mol^{-1}nm^{-2}$.

Atomistic simulations

Atomistic simulations were performed to characterize atomic interactions between $Na_v1.4$ residues and the bound $PI(4,5)P_2$ headgroup. Frames from a stable PIP2 binding event (from replicate 1 of enriched PIP simulations) were clustered using a selection of the bound PIP2 headgroup beads (C1 C2 C3 PO4 P1 P2) and binding residues K1329, K1330, K1333, K1463, K1466 and R1469 with an RMSD cutoff of 2.5 Å. The protein and bound PIP2 were extracted from the representative frame of the cluster and backbone beads of the coarse-grained VSD-IV were aligned to the corresponding carbon-alpha atoms in the original cryo-EM structure of $Na_v1.4$ (8). PIP2 was backmapped to atomistic coordinates of SAPI24 (the CHARMM lipid for $PI(4,5)P_2$ with -2e charge on P5, -1e charge on P4 and -1e on the PO4, as shown in **Fig 4D**) and the protein was replaced with the 6agf structure. The system was embedded in a 140 Å x 140 Å POPC membrane, solvated and 0.15 M NaCl added using the CHARMM-GUI Membrane Builder (39, 51, 52). An identical system was set up with $Na_v1.4$ in a POPC membrane without PIP.

Atomistic simulations were performed with Amber20 (53), using the CHARMM36m (54) and TIP3P water (55) forcefields. Equilibration steps were performed (minimization, heating, pressurizing), with 5 kJ/mol restraints on the protein backbone, followed by 24 ns of gradually reducing restraints. Five replicates of unrestrained production equilibrium simulations were performed, run for 1.5 μs each. The temperature was set at 310 K using the Langevin thermostat (56) and at a collision frequency of 5 ps^{-1}. Pressure was set at 1 bar using the Monte Carlo barostat (57) with anisotropic scaling and relaxation time of 1 ps. 12 Å van der Waals cut-off and hydrogen bond SHAKE constraints were used. Hydrogen mass repartitioning was used to enable a 4 fs timestep (58). $PI(4)P_1$ was also simulated with the same atomistic procedures, using the SAPI14 CHARMM lipid (with -2e charge on P4 and -1e on the PO4, as shown in **Fig 4D**).

Analysis

Coarse grain lipid-protein interactions were characterized using in-house python scripts which used the numpy, MDAnalysis (59) and pandas libraries (as done previously in Lin, Buyan and Corry (60)). A cut-off of 0.7 nm was used to define interactions between lipids and protein residues. Distance heatmaps were generated based on the minimum distance between a PIP bead and the side chain (SC2) bead of the arginine or lysine residue interacting. Binding durations were calculated by first counting the number of interactions between each PIP and VSD-IV binding residues (R1460, R1463, K1466 and R1469). A binding event is defined as the time between the first and last time that PIP interacts with two or more binding residues on VSD-IV, if it interacts with a minimum of one binding residue between this period. Stability of IFM/IQM motif binding in

flexible linker coarse-grained simulations was assessed by measuring the distance between the center of mass of the phenylalanine/glutamine residue to the center of mass of three residues (L1153, I1485 and N1591) within the IFM receptor site.

For atomistic simulations, MDAnalysis (59) was used to calculate RMSD of various parts of the protein and PIP headgroup, and RMSF of the carbon-alphas. Statistical significance in RMSF was assessed using student's t-test. ProLIF (61) was used to compute electrostatic interactions between the protein and binding residues. Representative snapshot of PIP2 binding was generated using the WMC Clustering Tool in VMD to identify the top cluster of the PIP2 headgroup (RMSD cutoff of 3 Å), then subsequently cluster the six binding residues to identify the most representative binding configuration. Trajectories were strided every 1 ns and the first 250 ns of simulations was discarded as equilibration time for analyses of RMSF, ProLIF interactions and clustering. All analysis scripts are available on *GitHub*.

Simulations were visualized and protein image figures produced using Visual Molecular Dynamics (VMD) (62). ClustalOmega (63, 64) and JalView (65) were used to generate and visualize sequence alignments. Structural representations of $K_V7.1$, $Ca_V2.2$ and $Na_V1.4$ structures were created in VMD by aligning each of the S4 helices on the VSD where the PIP was bound.

Acknowledgements

The authors thank Ruitao Jin for his contributions to the resting state homology model generation and comments on the manuscript draft. This research was undertaken with the assistance of resources and services from the National Computational Infrastructure (NCI), which is supported by the Australian Government. This research is also supported by Australian Government Research Training Program (RTP) Scholarships. Y.L. is supported by a 2023 NCI HPC-AI Talent Program Scholarship.

References

1. Yu F. H., Catterall W. A. (2003) **Overview of the voltage-gated sodium channel family** *Genome biology* **4**:1–7

2. Mantegazza M., Cestèle S., Catterall W. A. (2021) **Sodium channelopathies of skeletal muscle and brain** *Physiological Reviews* **101**:1633–1689

3. Venance S. L., et al. (2006) **The primary periodic paralyses: diagnosis, pathogenesis and treatment** *Brain* **129**:8–17

4. Jurkat-Rott K., et al. (2000) **Voltage-sensor sodium channel mutations cause hypokalemic periodic paralysis type 2 by enhanced inactivation and reduced current** *Proceedings of the National Academy of Sciences* **97**:9549–9554

5. Dib-Hajj S. D., Yang Y., Black J. A., Waxman S. G. (2013) **The NaV1. 7 sodium channel: from molecule to man** *Nature Reviews Neuroscience* **14**:49–62

6. Ghovanloo M.-R., et al. (2021) **Cannabidiol inhibits the skeletal muscle Nav1. 4 by blocking its pore and by altering membrane elasticity** *Journal of General Physiology* **153**

7. Ruiz M. de Lera, Kraus R. L. (2015) **Voltage-Gated Sodium Channels: Structure, Function, Pharmacology, and Clinical Indications** *Journal of Medicinal Chemistry* **58**:7093–7118

8. Pan X., et al. (2018) **Structure of the human voltage-gated sodium channel Nav1. 4 in complex with β1** *Science* **362**

9. El-Din T. M. Gamal, Lenaeus M. J., Zheng N., Catterall W. A. (2018) **Fenestrations control resting-state block of a voltage-gated sodium channel** *Proceedings of the National Academy of Sciences* **115**:13111–13116

10. Raju S., Barber A. F., LeBard D. N., Klein M. L., Carnevale V. (2013) **Exploring volatile general anesthetic binding to a closed membrane-bound bacterial voltage-gated sodium channel via computation** *PLoS computational biology* **9**

11. Boiteux C., Vorobyov I., Allen T. W. (2014) **Ion conduction and conformational flexibility of a bacterial voltage-gated sodium channel** *Proceedings of the National Academy of Sciences* **111**:3454–3459

12. Martin L. J., Corry B. (2014) **Locating the route of entry and binding sites of benzocaine and phenytoin in a bacterial voltage gated sodium channel** *PLoS computational biology* **10**

13. Tao E., Corry B. (2022) **Characterizing fenestration size in sodium channel subtypes and their accessibility to inhibitors** *Biophysical Journal* **121**:193–206

14. Clairfeuille T., et al. (2019) **Structural basis of α-scorpion toxin action on Nav channels** *Science* **363**

15. Cha A., Ruben P. C., George A. L., Fujimoto E., Bezanilla F. (1999) **Voltage sensors in domains III and IV, but not I and II, are immobilized by Na+ channel fast inactivation** *Neuron* **22**:73–87

16. Capes D. L., Goldschen-Ohm M. P., Arcisio-Miranda M., Bezanilla F., Chanda B. (2013) **Domain IV voltage-sensor movement is both sufficient and rate limiting for fast inactivation in sodium channels** *Journal of General Physiology* **142**:101–112

17. Goldschen-Ohm M. P., Capes D. L., Oelstrom K. M., Chanda B. (2013) **Multiple pore conformations driven by asynchronous movements of voltage sensors in a eukaryotic sodium channel** *Nature communications* **4**

18. Yan Z., et al. (2017) **Structure of the Nav1. 4-β1 complex from electric eel** *Cell* **170**:470–482

19. Hille B., Dickson E. J., Kruse M., Vivas O., Suh B.-C. (2015) **Phosphoinositides regulate ion channels** *Biochimica Et Biophysica Acta (BBA)-Molecular and Cell Biology of Lipids* **1851**:844–856

20. Sun J., MacKinnon R. (2020) **Structural basis of human KCNQ1 modulation and gating** *Cell* **180**:340–347

21. Gao S., Yao X., Yan N. (2021) **Structure of human Cav2. 2 channel blocked by the painkiller ziconotide** *Nature* **596**:143–147

22. Schmidt D., Jiang Q.-X., MacKinnon R. (2006) **Phospholipids and the origin of cationic gating charges in voltage sensors** *Nature* **444**:775–779

23. Kasimova M. A., Zaydman M. A., Cui J., Tarek M. (2015) **PIP2-dependent coupling is prominent in Kv7. 1 due to weakened interactions between S4-S5 and S6** *Scientific reports* **5**:1–9

24. Ma D., et al. (2022) **Structural mechanisms for the activation of human cardiac KCNQ1 channel by electro-mechanical coupling enhancers** *Proceedings of the National Academy of Sciences* **119**

25. Gada K. D., et al. (2023) **PI (4, 5) P2 regulates the gating of NaV1. 4 channels** *Journal of General Physiology* **155**

26. Liu Y., Jr C. A. Bassetto, Pinto B. I., Bezanilla F. (2023) **A mechanistic reinterpretation of fast inactivation in voltage-gated Na+ channels** *Nature communications* **14**

27. McPhee J. C., Ragsdale D. S., Scheuer T., Catterall W. A. (1998) **A critical role for the S4-S5 intracellular loop in domain IV of the sodium channel α-subunit in fast inactivation** *Journal of Biological Chemistry* **273**:1121–1129

28. West J. W., et al. (1992) **A cluster of hydrophobic amino acid residues required for fast Na (+)-channel inactivation** *Proceedings of the National Academy of Sciences* **89**:10910–10914

29. Mantegazza M., Yu F. H., Catterall W. A., Scheuer T. (2001) **Role of the C-terminal domain in inactivation of brain and cardiac sodium channels** *Proceedings of the National Academy of Sciences* **98**:15348–15353

30. Bezanilla F., Armstrong C. M. (1977) **Inactivation of the sodium channel. I. Sodium current experiments** *The Journal of general physiology* **70**

31. Zaman T., et al. (2018) **Mutations in SCN3A cause early infantile epileptic encephalopathy** *Annals of neurology* **83**:703–717

32. Frustaci A., et al. (2005) **Cardiac histological substrate in patients with clinical phenotype of Brugada syndrome** *Circulation* **112**:3680–3687

33. Liu Y., et al. (2020) **A PIP2 substitute mediates voltage sensor-pore coupling in KCNQ activation** *Communications biology* **3**

34. Mandala V. S., MacKinnon R. (2023) **The membrane electric field regulates the PIP2-binding site to gate the KCNQ1 channel** *Proceedings of the National Academy of Sciences* **120**

35. Corradi V., et al. (2018) **Lipid–protein interactions are unique fingerprints for membrane proteins** *ACS central science* **4**:709–717

36. Stansfeld P. J., Hopkinson R., Ashcroft F. M., Sansom M. S. (2009) **PIP2-binding site in Kir channels: definition by multiscale biomolecular simulations** *Biochemistry* **48**:10926–10933

37. Souza P. C., et al. (2021) **Martini 3: a general purpose force field for coarse-grained molecular dynamics** *Nature methods* **18**:382–388

38. Amsalem M., Poilbout C., Ferracci G., Delmas P., Padilla F. (2018) **Membrane cholesterol depletion as a trigger of Nav1. 9 channel-mediated inflammatory pain** *The EMBO journal* **37**

39. Jo S., Kim T., Iyer V. G., Im W. (2008) **CHARMM-GUI: a web-based graphical user interface for CHARMM** *Journal of computational chemistry* **29**:1859–1865

40. Qi Y., et al. (2015) **CHARMM-GUI martini maker for coarse-grained simulations with the martini force field** *Journal of chemical theory and computation* **11**:4486–4494

41. Wassenaar T. A., Ingólfsson H. I., Bockmann R. A., Tieleman D. P., Marrink S. J. (2015) **Computational lipidomics with insane: a versatile tool for generating custom membranes for molecular simulations** *Journal of chemical theory and computation* **11**:2144–2155

42. Ingólfsson H. I., et al. (2014) **Lipid organization of the plasma membrane** *Journal of the american chemical society* **136**:14554–14559

43. Shen H., Liu D., Wu K., Lei J., Yan N. (2019) **Structures of human Nav1. 7 channel in complex with auxiliary subunits and animal toxins** *Science* **363**:1303–1308

44. Šali A., Blundell T. L. (1993) **Comparative protein modelling by satisfaction of spatial restraints** *Journal of molecular biology* **234**:779–815

45. Huang G., et al. (2022) **Unwinding and spiral sliding of S4 and domain rotation of VSD during the electromechanical coupling in Nav1. 7** *Proceedings of the National Academy of Sciences* **119**

46. Wisedchaisri G., et al. (2021) **Structural basis for high-affinity trapping of the NaV1. 7 channel in its resting state by tarantula toxin** *Molecular cell* **81**:38–48

47. Bauer P., Hess B., Lindahl E. (2023) **GROMACS 2022.5 Manual (2022.5)**

48. de Jong D. H., et al. (2013) **Improved parameters for the martini coarse-grained protein force field** *Journal of chemical theory and computation* **9**:687–697

49. Evans D. J., Holian B. L. (1985) **The nose–hoover thermostat** *The Journal of chemical physics* **83**:4069–4074

50. Parrinello M., Rahman A. (1981) **Polymorphic transitions in single crystals: A new molecular dynamics method** *Journal of Applied physics* **52**:7182–7190

51. Wu E. L., et al. (2014) **CHARMM-GUI membrane builder toward realistic biological membrane simulations**

52. Lee J., et al. (2016) **CHARMM-GUI input generator for NAMD, GROMACS, AMBER, OpenMM, and CHARMM/OpenMM simulations using the CHARMM36 additive force field** *Journal of chemical theory and computation* **12**:405–413

53. Case D. A., et al. (2020) **AMBER 2020**

54. Huang J., et al. (2017) **CHARMM36m: an improved force field for folded and intrinsically disordered proteins** *Nature methods* **14**:71–73

55. Jorgensen W. L., Chandrasekhar J., Madura J. D., Impey R. W., Klein M. L. (1983) **Comparison of simple potential functions for simulating liquid water** *The Journal of chemical physics* **79**:926–935

56. Loncharich R. J., Brooks B. R., Pastor R. W. (1992) **Langevin dynamics of peptides: The frictional dependence of isomerization rates of N-acetylalanyl-N'-methylamide** *Biopolymers: Original Research on Biomolecules* **32**:523–535

57. Åqvist J., Wennerström P., Nervall M., Bjelic S., Brandsdal B. O. (2004) **Molecular dynamics simulations of water and biomolecules with a Monte Carlo constant pressure algorithm** *Chemical physics letters* **384**:288–294

58. Hopkins C. W., Le Grand S., Walker R. C., Roitberg A. E. (2015) **Long-time-step molecular dynamics through hydrogen mass repartitioning** *Journal of chemical theory and computation* **11**:1864–1874

59. Michaud-Agrawal N., Denning E. J., Woolf T. B., Beckstein O. (2011) **MDAnalysis: a toolkit for the analysis of molecular dynamics simulations** *Journal of computational chemistry* **32**:2319–2327

60. Lin Y. C., Buyan A., Corry B. (2022) **Characterizing the lipid fingerprint of the mechanosensitive channel Piezo2** *Biophysical Journal* **121**

61. Bouysset C., Fiorucci S. (2021) **ProLIF: a library to encode molecular interactions as fingerprints** *Journal of Cheminformatics* **13**:1–9

62. Humphrey W., Dalke A., Schulten K. (1996) **VMD: visual molecular dynamics** *Journal of molecular graphics* **14**:33–38

63. Goujon M., et al. (2010) **A new bioinformatics analysis tools framework at EMBL–EBI** *Nucleic acids research* **38**:W695–W699

64. Sievers F., et al. (2011) **Fast, scalable generation of high-quality protein multiple sequence alignments using Clustal Omega** *Molecular systems biology* **7**

65. Waterhouse A. M., Procter J. B., Martin D. M., Clamp M., Barton G. J. (2009) **Jalview Version 2—a multiple sequence alignment editor and analysis workbench** *Bioinformatics* **25**:1189–1191

Article and author information

Yiechang Lin
Research School of Biology, Australian National University, Canberra
For correspondence: yiechang.lin@anu.edu.au
ORCID iD: 0000-0001-9836-132X

Elaine Tao
Research School of Biology, Australian National University, Canberra
For correspondence: elaine.tao@anu.edu.au
ORCID iD: 0000-0003-0332-1646

James P Champion
Research School of Biology, Australian National University, Canberra

Ben Corry
Research School of Biology, Australian National University, Canberra
For correspondence: ben.corry@anu.edu.au
ORCID iD: 0000-0002-6324-442X

Copyright

Editors

Reviewing Editor
Toby Allen
RMIT University, Melbourne, Australia

Senior Editor
Merritt Maduke
Stanford University, Stanford, United States of America

Reviewer #1 (Public Review):

Summary: Here, the authors were attempting to use molecular simulation or probe the nature of how lipids, especially PIP lipids, bind to a medically-important ion channel. In particular, they look at how this binding impacts the function of the channel.

Strengths: The study is very well written and composed. The techniques are used appropriately, with plenty of sampling and analysis. The findings are compelling, and provide clear insights into the biology of the system.

Weaknesses: A few of the analyses are hard to understand/follow, and rely on "in house" scripts. This is particularly the case for the lipid binding events, which can be difficult to compute accurately. However the provision of these scripts on github means that these can be assessed by the reader if desired. Additionally, a lack of experimental validation, or coupling to existing experimental data, limits the study.

It is my view that the authors have achieved their aims, and their findings are compelling and believable. Their findings should have impacts on how researchers understand the functioning of the Nav1.4 channel, as well as on the study of other ion channels and how they interact with membrane lipids.

https://doi.org/10.7554/eLife.91218.2.sa2

Reviewer #2 (Public Review):

Summary:
Lin Y., Tao E., et al. used multiscale MD simulations to show that PI(4,5)P2 binds stably to an inactivated state of Nav channels at a conserved site within the DIV S4-S5 linker, which couples the voltage sensing domain (VSD) to the pore. The authors hypothesized that PI(4,5)P2 prolongs inactivation by binding to the same site where the C-terminal tail is proposed to bind during recovery from inactivation. They convincingly showed that PI(4,5)P2 reduces the mobility of both the DIV S4-S5 linker and the DIII-IV linker, thus slowing the conformational changes required for the channel to recover to the resting state. They also conducted MD simulations to show that phosphoinositides bind to VSD gating charges in the resting state of Nav channels. These interactions may anchor VDS at the resting state and impede its activation. Their results provide a mechanism by which phosphoinositides alter the voltage dependence of activation and the recovery rate from inactivation, an important step for developing novel therapies to treat Nav-related diseases. However, the study is incomplete lacks the expected confirmatory studies which are relevant to such proposals.

Strengths:
The authors identified a novel binding between phosphoinositides and the VSD of Nav and showed that the strength of this interaction is state-dependent. Based on their work, the affinity of PIPs to the inactivated state is higher than the resting state. This work will help pave the way for designing novel therapeutics that may help relieve pain or treat diseases like arrhythmia, which may result from a leftward shift of the channel's activation.

Weaknesses:
However, the study lacks the expected confirmatory studies relevant to such proposals. For example, one would expect that the authors would mutate the positive residues that they claim to make interactions with phosphoinositides to show that there are much fewer interactions once they make these mutations. Another point is that the authors found that the main interaction site of PIPs with Nav1.4 is the VSD-DIV and DIII-DIV linker. This interaction is expected to delay fast inactivation if it happens at the resting state. The authors should make a resting state model of the Nav1.4 channel to explain the recent experimental data showing that PIP2 delays the activation of Nav1.4, with almost no effect on the voltage dependence of fast inactivation.

The reviewers answered most of my concerns about the first version of the manuscript.

https://doi.org/10.7554/eLife.91218.2.sa1

Reviewer #3 (Public Review):

Summary:
This work uses multiscale molecular dynamics simulations to demonstrate molecular mechanism(s) for phosphatidylinositol regulation of voltage gated sodium channel (Nav1.4) gating. Recent experimental work by Gada et al. JGP 2023 showed altered Nav1.4 gating when Nav1.4 current was recorded with simultaneous application of PI(4,5)P2 dephosphorylate.

Here the authors revealed probable molecular mechanism that can explain PI(4,5)P2 modulation of Nav1.4 gating. They found PIP lipids interacting with the gating charges - potentially making it harder to move the voltage sensor domain and altering the channels voltage sensitivity. They also found a stable PIP binding site that reaches the D_IV S4-S5 linker, reducing the mobility of the linker and potentially competing with the C-terminal domain.

Strengths:
Using multiscale simulations with course-grained simulations to capture lipid-protein interactions and the overall protein lipid fingerprint and then all-atom simulations to verify atomistic details for specific lipid-protein interactions is extremely appropriate for the question at hand. Overall, the types of simulation and their length are suitable for the questions the authors pose and a thorough set of analysis was done which illustrates the observed PIP-protein interactions.

Weaknesses:
Although the set of current simulations and analysis supports the conclusions drawn nicely, the course-grained simulations have further utility than that utilized by the authors. With the 4to1 heavy atoms bead mapping in Martini 2 some detailed chemical specificity is averaged out but parameters for different PIP family members do exist - including specific PIP(4,5)P2 vs PIP(3,4)P2, and could have been explored at the course-grained level. However, performing more detailed all-atom simulation, as done in this manuscript, is always advisable to extend and/or confirm course-grained results.

https://doi.org/10.7554/eLife.91218.2.sa0

Author Response

The following is the authors' response to the original reviews.

We thank the reviewers for their thorough reading and helpful comments which has allowed us to further improve the manuscript. Following the suggestions of the reviewers we have run a number of new simulations including mutations of the PIP binding residues and with an elastic network allowing more mobility of the linker. Together these excellent ideas have allowed us to strengthen the conclusions of the study. Below, we provide point-by-point responses to their suggestions.

> ***Reviewer #1 (Public Review):***
>
> *Summary:*
>
> *Here, the authors were attempting to use molecular simulation or probe the nature of how lipids, especially PIP lipids, bind to a medically-important ion channel. In particular, they look at how this binding impact the function of the channel.*
>
> *Strengths:*
>
> *The study is very well written and composed. The techniques are used appropriately, with plenty of sampling and analysis. The findings are compelling and provide clear insights into the biology of the system.*
>
> *Weaknesses:*
>
> *A few of the analyses are hard to understand/follow, and rely on "in house" scripts. This is particularly the case for the lipid binding events, which can be difficult to compute*

> *accurately. Additionally, a lack of experimental validation, or coupling to existing experimental data, limits the study.*

Our analysis scripts have now been made publicly accessible as a Jupyter notebook on Github https://github.com/etaoster/etaoster.github.io/tree/main/nav_pip_project

> *It is my view that the authors have achieved their aims, and their findings are compelling and believable. Their findings should have impacts on how researchers understand the functioning of the Nav1.4 channel, as well as on the study of other ion channels and how they interact with membrane lipids.*
>
> ***Reviewer #2 (Public Review):***
>
> *Summary:*
>
> *Y., Tao E., et al. used multiscale MD simulations to show that PI(4,5)P2 binds stably to an inactivated state of Nav channels at a conserved site within the DIV S4-S5 linker, which couples the voltage sensing domain (VSD) to the pore. The authors hypothesized that PI(4,5)P2 prolongs inactivation by binding to the same site where the C-terminal tail is proposed to bind during recovery from inactivation. They convincingly showed that PI(4,5)P2 reduces the mobility of both the DIV S4-S5 linker and the DIII-IV linker, thus slowing the conformational changes required for the channel to recover to the resting state. They also conducted MD simulations to show that phosphoinositides bind to VSD gating charges in the resting state of Nav channels. These interactions may anchor VDS at the resting state and impede its activation. Their results provide a mechanism by which phosphoinositides alter the voltage dependence of activation and the recovery rate from inactivation, an important step for developing novel therapies to treat Nav-related diseases. However, the study is incomplete and lacks the expected confirmatory studies which are relevant to such proposals.*
>
> *Strengths:*
>
> *The authors identified a novel binding between phosphoinositides and the VSD of Nav and showed that the strength of this interaction is state-dependent. Based on their work, the affinity of PIPs to the inactivated state is higher than the resting state. This work will help pave the way for designing novel therapeutics that may help relieve pain or treat diseases like arrhythmia, which may result from a leftward shift of the channel's activation.*
>
> *Weaknesses:*
>
> *However, the study lacks the expected confirmatory studies which are relevant to such proposals. For example, one would expect that the authors would mutate the positive residues that they claim to make interactions with phosphoinositides to show that there are much fewer interactions once they make these mutations. Another point is that the authors found that the main interaction site of PIPs with Nav1.4 is the VSD-DIV and DIII-DIV linker, an interaction that is expected to delay fast inactivation if it happens at the resting state. The authors should make a resting state model of the Nav1.4 channel to explain the recent experimental data showing that PIP2 delays the activation of Nav1.4, with almost no effect on the voltage dependence of fast inactivation.*

Following the reviewers suggestion we have conducted new simulations demonstrating that there are many fewer protein-PIP interactions after mutating the positive residues as shown in the new Supplementary Fig S6.

The reviewer mentions that if PIPs interact with the VSD-DIV and DIII-DIV linker in the resting state that it could delay fast inactivation. However, as described in the original

manuscript and depicted in the schematic (Fig 7) the C-terminal domain impeded PIP binding at the position in the resting state (but not the inactivated state), meaning that PIP does not bind in the resting state to delay fast inactivation. We have clarified this statement in the text on page 14 lines 1-2.

Following the reviewer's suggestion we have examined PIP binding to a model of the resting state of Nav1.4 (in addition to the resting state of Nav1.7 described in the original manuscript) as described on page 12 lines 28-30 (and in Fig S12). Similar to what we saw for Nav1.7, PIP binding to VSDI-III can impair activation of the channel.

> *Major concern:*
>
> *(1) Lack of confirmatory experiments, e.g., mutating the positive residues that show a high affinity towards PIPs to a neutral and negative residue and assessing the effect of mutagenesis on binding.*

Done as described above

> *(2) Nav1.4 is the only channel that has been studied in terms of the effect of PIPs on it, therefore the authors should build a resting state model of Nav1.4 and study the effect of PIPs on it.*

Done as described above

> *Minor points:*
>
> *There are a lot of wrong statements in many areas, e.g., "These diseases 335 are associated with accelerated rates of channel recovery from inactivation, consistent with our observations that an interaction between PI(4,5)P2 and the residue corresponding to R1469 in other Nav 337 subtypes could be important for prolonging the fast-inactivated state." Prolonging the fast inactivated state would actually reduce recovery from inactivation and not accelerate it.*

We disagree with this statement from the reviewer which may have come from a misreading of the mentioned sentence. Our statement in the original manuscript is consistent with the original experiments that show that the presence of PIP prolongs the time spent in the fast inactivated state. Mutations at the PIP binding site are likely to reduce PIP binding, and with less PIP bound the channel is expected to recover from inactivation more quickly. We have reworded this sentence for clarity on page 13 line 27-30.

> ***Reviewer #3 (Public Review):***
>
> *Summary:*
>
> *This work uses multiscale molecular dynamics simulations to demonstrate molecular mechanism(s) for phosphatidylinositol regulation of voltage gated sodium channel (Nav1.4) gating. Recent experimental work by Gada et al. JGP 2023 showed altered Nav1.4 gating when Nav1.4 current was recorded with simultaneous application of PI(4,5)P2 dephosphorylate. Here the authors revealed probable molecular mechanism that can explain PI(4,5)P2 modulation of Nav1.4 gating. They found PIP lipids interacting with the gating charges - potentially making it harder to move the voltage sensor domain and altering the channels voltage sensitivity. They also found a stable PIP binding site that reaches the D_IV S4-S5 linker, reducing the mobility of the linker and potentially competing with the C-terminal domain.*
>
> *Strengths:*

> *Using multiscale simulations with course-grained simulations to capture lipid-protein interactions and the overall protein lipid fingerprint and then all-atom simulations to verify atomistic details for specific lipidprotein interactions is extremely appropriate for the question at hand. Overall, the types of simulation and their length are suitable for the questions the authors pose and a thorough set of analysis was done which illustrates the observed PIP-protein interactions.*
>
> *Weaknesses:*
>
> *Although the set of current simulations and analysis supports the conclusions drawn nicely, there are some limitations imposed by the authors on the course-grained simulations. If those were not imposed, it would have allowed for an even richer set and more thorough exploration of the protein-lipid interactions. The Martini 2 force field indeed cannot change secondary structure but if run with a properly tuned elastic network instead of backbone restraints, the change in protein configuration can be sampled and/or some adaptation of the protein to the specific protein environment can be observed. Additionally, with the 4to1 heavy atoms to a bead mapping some detailed chemical specificity is averaged out but parameters for different PIP family members do exist - including specific PIP(4,5)P2 vs PIP(3,4)P2, and could have been explored.*

We thank the reviewer for their excellent suggestions and have run new simulations with an elastic network instead of backbone restraints which have generated new insights. Indeed, as shown in the new panel Fig 4E, the new data allows us to demonstrate that the presence of PIP in the proposed binding site stabilises binding of the DIII-DIV linker to the inactivation receptor site, strengthening the conclusions of the paper.

We thank the reviewer for pointing out that there do exist parameters for different PIP sub-species and have corrected our statement on page 14 line 16 to reflect this. We have not run additional CG simulations with each of these parameters but use the all-atom simulations to examine the interactions of phosphates at specific positions.

In our atomistic simulations, we backmapped both PI(4,5)P2 and PI(4)P in the binding site to study their specific interactions. We chose to focus on PI(4,5)P2 given its physiological significance. However, we agree that differences in binding with PI(3,4)P2 would be interesting and warrants future investigation. We also note that the newer Martini3 forcefield would be useful in further work to differentiate between PIP subspecies interactions.

> *Detailed Comments*

We thank the reviewers for their thorough reading and helpful comments which has allowed us to further strengthen the manuscript. Below, we provide point-by-point responses to their suggestions.

> ***Reviewer #1 (Recommendations For The Authors):***
>
> *I don't have many suggestions for the manuscript, just a few text edits. Of course, experimental analysis would bolster the claims made in the text, but I don't believe that this is necessary, given the quality of the data.*
>
> *I understand the focus on the PIP lipids, but it's a shame that the high binding likelihood of glycosphingolipid isn't considered or analysed in any way. This is an especially interesting lipid from the point-of-view of raftlike membrane domains. Given the potential role of raft-like domains in sodium channel function, I feel this would be worth a paragraph or two in the discussion.*

We thank the reviewer for bringing our attention to this interesting point. Glycolipids accumulate around Nav1.4 in our complex membrane simulations, however, given reports that carbohydrates tend to interact too strongly in the Martini2.2 forcefield (Grünewald et al. 2022, Schmalhorst et al. 2017) and there are no specific residues on Nav1.4 that interact preferentially with glycolipid species, we chose not to focus on this. However, we have noted that interactions with other lipids deserve further attention in our revised discussion.

> *The analyses have been run using Martini 2. I don't suggest the authors repeat using the Martini 3 force field, but some mention of this in the discussion would be good.*

We have added the following statement to the discussion: “Our coarse grain simulations were carried out using the Martini2.2 forcefield, for which lipid parameters for many plasma membrane lipids have been developed. We expect that future investigations of lipid-protein interactions will benefit from use of the newer, refined Martini 3 forcefield (Souza et al. 2021) as parameters become available for more lipid types.

> *This might just be an oversight, but no mention is made of an elastic network applied to the backbone beads.*
>
> *Lack of a network has been known to cause the protein to collapse, so if this is missing, I'd like to see an RMSD to show that the protein dynamics are not compromised.*

While no elastic network was used in our original CG simulations, weak protein backbone restraints (10 kJ mol-1 nm-2) used in our simulations allowed us to maintain the structure while allowing some protein movement. However, following the suggestion of reviewer 3, we conducted additional simulations with an elastic instead of backbone restraints as described in the results on page 9 line 30-37 (and in Fig 4E) of the revised manuscript.

> *Minor*
>
> *•In Fig 3B, are these lipids binding to the channel at the same time? And therefore do the authors see cooperativity?*

The Fig 3B caption has been amended in the revised manuscript to read “Representative snapshots from the five longest binding events from different replicates, showing the three different PIP species (PIP1 in blue, PIP2 in purple and PIP3 in pink) binding to VSD-IV and the DIII-IV linker.” We cannot comment on PIP cooperativity based on these simulations shown in Fig 3, due to the artificially high concentrations used here; however, in model complex membrane simulations we see co-binding of PIPs at the binding site. This is likely due to PIP’s ability to accumulate together and the high density of positively charged residues in the region, attracting and supporting multiple PIP bindings.

> *•What charges were used for the atomistic PIP lipids? Does this match the CG lipids?*

We used the CHARMM-GUI PIP parameters for the atomistic simulations. SAPI24 (PIP2) has a headgroup charge of –4e which is one less negative charge than the CG PIP2; whereas SAPI14 (PIP1) has a charge of –3e which is the same as the CG PIP1. We have explicitly included this charge information in the updated Methods of the manuscript (on page 15-16).

> *•Line 259-260: "we performed embedded three structures"*

Corrected in the revised manuscript.

> *•Line 272: "us" should be "μs"*

Corrected in the revised manuscript.

> *•Line 434: kJ/mol should probably also have 'nm-2' included*

Corrected in the revised manuscript.

> *•What charge state titratable residues were set to, and were pKa analyses done to decide this?*

Charge states were assigned to default values at neutral pH. We appreciate that future studies could examine this more carefully using constant pH simulations or similar.

> *•It's stated that anisotropic scaling is used the AT sims - is this correct? If so, is there a reason this was chosen over semi-isotropic scaling?*

Anisotropic scaling was used for the atomistic simulations allowing all box dimensions to change independently.

> *•I would recommend in-house analysis scripts are made available on GitHub or similar, just so the details can be seen.*

Per the reviewer's request, the Jupyter notebooks used for analysis has been made available on GitHub (https://github.com/etaoster/etaoster.github.io/tree/main/nav_pip_project).
-One coarse grained notebook:

- Lipid DE
- Contact occupancy + outlier plots
- Binding duration plots
- Minimum distance plots
- Number of ARG/LYS plots
- PIP Occupancy, binding duration, gating charge residues
- One atomistic notebook:
- RMSD, RMSF and distance between IFM and its binding pocket (using MDAnalysis)
- Atomistic PIP headgroup interaction analyses and plots (using ProLIF)

> *As a final note, I am* NOT *saying this needs to be done for the current study, but I recommend the authors try the PyLipID package (https://github.com/wlsong/PyLipID) if they haven't yet, as it might be useful for similar projects they run in the future (i.e. for binding site identification, accurate binding kinetics calculations, lipid pose generation etc.).*

We thank the reviewer for this suggestion and will keep this in mind for future projects.

> ***Reviewer #2 (Recommendations For The Authors):***
>
> *Lin Y., Tao E., et al. used multiscale MD simulations to show that PI(4,5)P2 binds stably to an inactivated state of Nav channels at a conserved site within the DIV S4-S5 linker, which couples the voltage sensing domain (VSD) to the pore. The authors hypothesized that*

> *PI(4,5)P2 prolongs inactivation by binding to the same site where the C-terminal tail is proposed to bind during recovery from inactivation. They convincingly showed that PI(4,5)P2 reduces the mobility of both the DIV S4-S5 linker and the DIII-IV linker, thus slowing the conformational changes required for the channel to recover to the resting state. They also conducted MD simulations to show that phosphoinositides bind to VSD gating charges in the resting state of Nav channels. These interactions may anchor VDS at the resting state and impede its activation. Their results provide a mechanism by which phosphoinositides alter the voltage dependence of activation and the recovery rate from inactivation, an important step for developing novel therapies to treat Nav-related diseases. However, the study is incomplete lacks the expected confirmatory studies which are relevant to such proposals.*
>
> *The authors identified a novel binding between phosphoinositides and the VSD of Nav and showed that the strength of this interaction is state-dependent. Based on their work, the affinity of PIPs to the inactivated state is higher than the resting state. This work will help pave the way for designing novel therapeutics that may help relieve pain or treat diseases like arrhythmia, which may result from a leftward shift of the channel's activation. However, the study lacks the expected confirmatory studies which are relevant to such proposals. For example, one would expect that the authors would mutate the positive residues that they claim to make interactions with phosphoinositides to show that there are much fewer interactions once they make these mutations. Another point is that the authors found that the main interaction site of PIPs with Nav1.4 is the VSD-DIV and DIII-DIV linker, an interaction that is expected to delay fast inactivation if it happens at the resting state. The authors should make a resting state model of the Nav1.4 channel to explain the recent experimental data showing that PIP2 delays the activation of Nav1.4, with almost no effect on the voltage dependence of fast inactivation.*
>
> *Major concern:*
>
> *(1) Lack of confirmatory experiments, e.g., mutating the positive residues that show a high affinity towards PIPs to a neutral and negative residue and assessing the effect of mutagenesis on binding.*
>
> *(2) Nav1.4 is the only channel that has been studied in terms of the effect of PIPs on it, therefore the authors should build a resting state model of Nav1.4 and study the effect of PIPs on it. Minor points:*

Following the reviewer's suggestion we have conducted new simulations demonstrating that there are notably fewer protein-PIP interactions after performing charge neutralizing and charge reversal mutations to the positive residues as shown in the new Fig S6.

The reviewer mentions that if PIPs interact with the VSD-DIV and DIII-DIV linker in the resting state that it could delay fast inactivation. However as described in the original manuscript and depicted in the schematic (Fig 7) the C-terminal domain impeded PIP binding at the position in the resting state (but not the inactivated state), meaning that PIP does not bind in the resting state to delay fast inactivation. We have clarified this statement in the text on page 14 lines 1-2.

Following the reviewers suggestion we have examined PIP binding to a model of the resting state of Nav1.4 (in addition to the resting state of Nav1.7 described in the original manuscript) as described on page 12 lines 28-30 (and in Fig S12). Similar to what we saw for Nav1.7 PIP binding to VSDI-III can impair activation of the channel.

> *There are a lot of wrong statements in many areas, e.g., "These diseases 335 are associated with accelerated rates of channel recovery from inactivation, consistent with our observations that an interaction between PI(4,5)P2 and the residue corresponding to*

> *R1469 in other Nav 337 subtypes could be important for prolonging the fast-inactivated state." Prolonging the fast inactivated state would actually reduce recovery from inactivation and not accelerate it.*

We disagree with this statement from the reviewer which may have come from a misreading of the mentioned sentence. Our statement in the original manuscript is consistent with the the original experiments that show that the presence of PIP prolongs the time spent in the fast inactivated state. Mutations at the PIP binding site are likely to reduce PIP binding, and with less PIP present the channel will recover from inactivation more quickly. We have reworded this sentence for clarity on page 13 line 27-30.

> ***Reviewer #3 (Recommendations For The Authors):***
>
> *As mentioned in the public review, overall, I am impressed with the manuscript and do think the conclusions are supported. There are, however, quite a few mistakes, mostly minor (listed below). Additionally, I do have a few questions and several extensions that could be done and I mention a few but fully realize many of those could be outside of the scope of the current manuscript.*

We greatly appreciate the time taken by Reviewer 3 to carefully review our manuscript and provide detailed comments. We believe their suggestions have helped to improve our manuscript.

> *First comments are in general about the PIP subtype.*
>
> - *In the paper you claim:*
>
> *L196, "However, this loss of resolution prevents distinction between phosphate positions on the inositol group and does not permit analysis of protein conformational changes induced by PIP binding"*
>
> *L367, "it does not distinguish between phosphate positions within each charge state (e.g. PI(3,4)P2 vs PI(4,5)P2)."*
>
> *This is not true the PIP2 most commonly used in Martini 2 is from dx.doi.org/10.1021/ct3009655 and is a PI(3,4)P2 subtype. Also other extensions and alternative parameters exist for PIPs in Martini 2 e.g. http://cgmartini.nl/index.php/tools2/other-tools - Martini lipid .itp generator has all three main variants of both PIP1 and PIP2.*

As described in the response to the public review we are grateful for the reviewer for pointing out that there do exist parameters for different PIP sub-species and have corrected our statement on page 14 to reflect this, and clarified the parameters chosen in the methods section (page 16 line 2-3). We have not run additional CG simulations with each of these parameters in the current work but use the all-atom simulations to examine the interactions of phosphates at specific positions.

> - *One detail that is missing in the manuscript is some mention of the charge state of the PIPs e.g. Fig.1D does not specify and Fig.4D PIP2 looks like -2 on position 5 and -1 on position 4. Which I think fits the used SAPI24, please specify. Also, what if you use SAPI25 with the flipped charges would that significantly alter the results?*

The charge state of PIP2 is -2e on the 5' phosphate and -1e on the 4' phosphate, using the SAPI24 CHARMM lipid parameters. We have ensured that this charge information is stated clearly in the revised manuscript in the methods section on page 16 (line 21). We considered looking at SAPI25, however we expected that it would behave quite similarly, given that the PIP headgroup can adopt slightly different poses and orientations within the binding site across replicates and does fluctuate over simulations (Fig S8). We have noted this in the revised discussion on page 14 line 15-17.

> - *I was very intrigued and puzzled by the lower binding of PIP3 vs PIP2 in the Martini simulations. Could it be that PIP3 has a harder time fully entering the binding site, or maybe just sampling? i.e. and its lower number of binding events is a sampling issue.*

We agree with the reviewer that PIP3 is less able to access the binding site than PIP2, likely because of its larger size. This might also be why we see PIP1 binding at the location via a more buried route (since it has the smallest headgroup size). However, PIP1 does not have enough negative charge to keep it in the binding site. It seems to be a Goldilocks-like situation where PIP2 has the optimal size and charge to allow access and stable binding at the site. We also see that when PIP3 enters the binding site it leaves before the end of the simulations. While it is hard to prove statistical significance given the number of binding and dissociation events even with the high and equal concentrations of all three PIP species in the enriched PIP membrane CG simulations, the data strongly suggests preferential binding of PIP2 over PIP3.

> *Also the same L196 sentence as above "However, this loss of resolution prevents distinction between phosphate positions on the inositol group and does not permit analysis of protein conformational changes induced by PIP binding". The later part is also wrong, there are no conformational changes due to the restraints on the protein backbone, from methods "backbone beads were weakly restrained to their starting coordinates using a force constant of 10 kJ mol−1nm−2". Martini in general might have a hard time with some conformational changes and definitely cannot sample changes in secondary structure, but conformational changes can, and have on many occasions, been successfully sampled (even full ion channel opening and closing).*
>
> *On a similar note, in L179 you mention "owing to the flexibility of the linker." Hose does this fit with simulation with position restraints on all backbone atoms?*

We applied fairly weak restraints to the backbone only – therefore we still observe some flexibility in the highly flexible loop portion of the linker, where sidechains are able to flip between membrane-facing and cytosol-facing orientations.

However, after reading the comments from the reviewer we have run additional simulations with an elastic network rather than backbone restraints on the DIII-DIV linker which have given further insight. As seen in Fig 4E and described in the results paragraph on page 9 line 30-37 of the revised manuscript, we can see that the presence of PIP does stabilise the linker in its receptor site. To accentuate this effect, we also ran simulation of the 'IQM' mutant known to have a less stable fast inactivated state due to weaker binding to the receptor. Without backbone restraints we can see partial dissociation of the DIII-DIV linker from the receptor that is partially rescued by the presence of PIP.

> *I know the paper focuses on PIPs, also very nicely in Fig.2B and Fig. S1-2 the lipid enrichment is shown for other lipids, but why show all lipid classes except cholesterol? And, for the left-hand panels in Fig. S1-2 those really should be leaflet specific - as both the membrane and protein are asymmetric.*

The depletion/enrichment of Cholesterol is shown in Fig 2B and as are the Lipid Z-Density maps and contact occupancy structures a (in row 5 of Fig S2, labeled as CL in yellow). The Z-density maps are meant to provide an overall summary of lipid distribution. The contact occupancy structures showing the transverse views and intracellular/ extracellular views provide a better indication of the occupancy across the different leaflets.

> *In L237 for the comparison of Cav2.2 and Kv7.1 bound to PI(4,5)P2 structures: They do agree well with the PIP1 simulations but not as much for the main PIP2 binding site. If you look in the CG simulations, is there another (not the main) PIP2 binding site at that same location (which might also be stable in AA simulations)?*

In some replicates of the CG simulations, we identify stable PIP1 binding via the other orientation (i.e. the one that overlaps with the Cav2.2 and Kv7.1 structures). Since we did not directly observe any PIP2 binding events from the other orientation, we did not run any backmapped atomistic simulations with PIP2 at this position. However, the binding site residues that the PIP1/2 headgroup binds to are the same regardless of which side PIP1/2 approaches from. We would expect that PIP2 bound from the alterative position is also stable.

> *Two references I want to put for consideration to the authors, for potential inclusion if the authors find their inclusion would strengthen the manuscript. This one gives a good demonstration of using the same PM mixture to define lipid protein fingerprints with Martini:*
>
> *https://pubs.acs.org/doi/10.1021/acscentsci.8b00143.*
>
> *And this one https://pubmed.ncbi.nlm.nih.gov/33836525/ shows how Nav1.4 function could also be affected by general changes in bilayer properties (in addition to the specific lipid interactions explored here).*

We thank the reviewer for bringing to our attention these two relevant references that will help to respectively substantiate the use Martini to study membrane protein-lipid interactions, as well as, why Nav channels are interesting to study in the context of their membrane environment (and also the potential implications with drugs that can bind from within the membrane). We have added these citations to the introduction and discussion.

> *Minor comments and fixes:*
>
> *L2, Title: A binding site for phosphoinositide modulation of voltage-gated sodium channels described by multiscale simulations*
>
> *The title reads very strangely to me, should it be "A binding site for phosphoinositide" ; "modulation". We thank the reviewer for this comment - title has been updated to: A binding site for phosphoinositides described by multiscale simulations explains their modulation of voltage gated sodium channels.*
>
> *L25, Abstract, "The phosphoinositide PI(4,5)P2 decreases Nav1.4 activity by increasing the difficulty of channel opening, accelerating fast activation and slowing recovery from fast inactivation." Assuming this is referring to results from Gada et al JGP, 2023 should this not be "accelerating fast inactivation"?*

Corrected in the revised manuscript.

> *L71 maybe good to write the longer version of IFM on first use e.g. Ile-Phe-Met (IFM), as to not mistake it for some random three letter acronym.*

Corrected in the revised manuscript.

> *L109, Fig.2. Maybe change the upper and lower leaflet to intracellular and cytoplasmic leaflets (or outer / inner). In D "(D) Distribution of PIP binding occupancies (left)" something missing can I assume, for/over all lipids exposed residues. Also, for D I am a little confused how occupancy is defined as the total occupancy per residue dose not add up to 100.*

The figure has been updated with intracellular and cytoplasmic leaflet labels. The binding occupancy distribution boxplot shows binding occupancies for all lipid exposed residues. In our analysis, we define contact occupancy as the proportion of simulation time in which a lipid type is within 0.7 nm of a given residue. It is possible for more than one lipid to be within this cut in any given frame – that is, both a PIP and PE can be simultaneously bound.

> *L160 "occurring the identified site" in the*

Corrected in the revised manuscript.

> *L170 "PIP3 (headgroup charge: -7e) has interacts similarly to PIP1," - remove has Corrected in the revised manuscript.*
>
> *L194, "reducing system size" the size does not change, I am assuming you want to say reducing the number of particles?*

Corrected in the revised manuscript.

> *L252, Fig.6 "(B) Occupancy of all PIPs (PIP1, PIP2, PIP3) at binding site residues in the three systems" A little confusing, initially was expecting 3x3 data points per residue, maybe change to, Combined occupancy of all PIPs...*

Corrected in the revised manuscript.

> *L253, Fig.6 D, I don't really have a good suggestion for improvement here, so this is just a FYI that this panel was very confusing for me and took some time to figure out what is shown.*

We have added to the caption of Fig. 6D to try to clarify this panel.

> *L257, Fig.6 (F) not in bold*

Corrected in the revised manuscript.

> *L259 "PIP binding, we performed embedded three structures of Nav1.7" something missing?*

Corrected in the revised manuscript.

> *L272, "In triplicate 50 us coarse-grained simulations" us instead of (micro_greek)s*

Corrected in the revised manuscript.

> *L272, that paragraph how long/many simulations only reported for the inactivated Nav1.7 system not the Nav1.7-NavPas chimera, which I am assuming is the same?*

Corrected in the revised manuscript.

> *L297, "marked by both shortened inactivation times", can I assume this is: shortened times to inactivation (i.e. to get inactivated not times in the inactivated states)?*

Corrected in the revised manuscript.

> *L331, "are conserved in Nav1.1-1.9 (Fig. 5D)," Fig.5C Corrected in the revised manuscript.*
>
> *L353, "channel opening []" [] maybe a missing reference?*

Thank you for pointing out this oversight - Goldschen-Ohm et al. has been cited here.

> *L394, "The composition of the complex mammalian membrane is as reported in Ingólfsson, et al. (38)." Ref 38 is the "Computational lipidomics of the neuronal plasma membrane" which indeed uses the 63 component PM but the original reference for the average 63 lipid mixture PM is dx.doi.org/10.1021/ja507832e.*

Corrected in the revised manuscript.

> *L404, "Additionally, a model Nav1.7 with all four VSDs in the deactivated state using Modeller (40)." Something missing, e.g. was also built and simulated for ...*

Corrected in the revised manuscript.

> *Table S1 "Disease information", I am guessing this should be Disease information; mechanism? Of the x5 entries two have mechanism, one has "; unknown significance ", one has "; unknown" maybe clarify in title and make same if unknown.*

Corrected in the revised manuscript.

> *Table S1 and S2 have different styles.*

The tables have been amended to have the same style.

> *Fig. S3 "for all 12 lipid types in the mammalian membrane " there are many more lipid types in a typical PM (hundreds) and 63 in the PM mixture simulated here, so maybe write: 12 lipid classes?*

Corrected in the revised manuscript.

> *Fig.S6 PIP headgroup, can I assume that is for the bound PIP only, please specify.*

Only a single PIP at the identified binding site was backmapped into all cases of atomistic simulations. We have now clarified this point in the methods, results and the FigS6 caption.

> *Writing of PI(4,5)P2 and PI(4)P1 most of the time use 1 and 2 as subscripts but not always (at least not in SI), also the same with Nav vs Na_v (v subscript) and even NAV (in Table S1).*

Subscripts have been implemented in the updated Supplementary Information (as well as within various figures and throughout the manuscript).